Title
Polar growth and cell division in Agrobacterium tumefaciens

Author
Anderson-Furgeson, James Christian

Publication Date
2016

Peer reviewed|Thesis/dissertation

Polar growth and cell division in *Agrobacterium tumefaciens*

By

James Christian Anderson-Furgeson

A dissertation submitted in partial satisfaction of the requirements for the degree of

Doctor of Philosophy

In

Microbiology

In the Graduate Division of the

University of California, Berkeley

Committee in charge:

Professor Patricia C. Zambryski, chair

Professor Kathleen Ryan, inside

Professor Arash Komeili, inside

Professor David Drubin, outside

Spring 2016

Abstract

Polar growth and cell division in *Agrobacterium tumefaciens*

by

James Christian Anderson-Furgeson

Doctor of Philosophy in Microbial Biology

University of California, Berkeley

Professor Patricia C Zambryski, Chair

Agrobacterium tumefaciens is a rod-shaped gram-negative bacterium, which elongates by unipolar addition of new cell envelope material. Approaching cell division, the growth pole transitions to a non-growing old pole, and the division site creates new growth poles in sibling cells. This thesis describes experiments concerning cell division and polar growth in *A. tumefaciens.* The cell division proteins FtsZ-GFP and FtsA-GFP localize to the growth pole in addition to the Z-ring at the mid-cell. The *A. tumefaciens* homolog of the *Caulobacter crescentus* polar organizing protein $PopZ_{Cc}$ ($PopZ_{At}$) localizes specifically to growth poles. In contrast, the *A. tumefaciens* homolog of the *C. crescentus* polar organelle development protein $PodJ_{Cc}$ ($PodJ_{At}$) localizes to the old pole early in the cell cycle and accumulates at the growth pole as the cell cycle proceeds. FtsA and FtsZ also localize to the growth pole for most of the cell cycle prior to Z-ring formation. To further characterize the function of polar localizing proteins, I created a deletion of $podJ_{At}$. $\Delta podJ_{At}$ cells display ectopic growth poles (branching), growth poles that fail to transition to an old pole, and elongated cells that fail to divide. In $\Delta podJ_{At}$ cells, $PopZ_{At}$-GFP persists at non-transitioning growth poles post division and also localizes to ectopic growth poles, as expected for a growth pole specific factor. Even though GFP-$PodJ_{At}$ does not localize to the midcell in wild type, deletion of $podJ_{At}$ impacts localization, stability, and function of Z-rings as assayed by localization of FtsA-GFP and FtsZ-GFP. Z-ring defects are further evidenced by minicell production. Together these data indicate that $PodJ_{At}$ is a critical factor for polar growth, and $\Delta podJ_{At}$ displays a cell division phenotype. These results reveal intimate connections between polar growth and cell division in a model system displaying a novel form of cell growth.

TABLE OF CONTENTS

FIGURES INDEX

TABLES INDEX

DEDICATION

I would like to dedicate this thesis to my parents, Barbara Anderson and Jim Furgeson, my brothers, Will Furgeson and Andy Furgeson, my sisters-in-law, Jessie Grace Eller-Isaacs and Casey Miller, my nephew Lewis, and to the memories of my grandparents, Vera Ann Anderson, Roland Anderson, Alyene Furgeson, and Royal Furgeson. I would also like to dedicate this thesis to my partner, Susanna Davy.

ACKNOWLEDGEMENTS

Without the help of the people listed here, writing this dissertation would not have been possible.

I thank my advisor and mentor, Patricia Zambryski. I also thank the co-authors on the $\Delta podJ_{At}$ paper, John Zupan and Romain Grangeon. I would like to acknowledge my lab-mates Howard Goodman, Jake Brunkard, and Anne Runkel, who all gave valuable insights.

I would also like to thank my thesis committee, Professors David Drubin, Arash Komeili, and Kathleen Ryan for their guidance. Professor Steve Lindow, who was a committee member on my Qualifying Exam, and Professor Peggy Lemaux both provided guidance through grad school.

Steve Ruzin, PhD, and Denise Schichnes, PhD, of the Biological Imaging Facility gave invaluable help with the light microscopy reported in this manuscript. Similarly, the electron microscopy performed here would not have been possible without help from Guangwei Min, PhD, of the Electron Microscopy Lab at UC Berkeley.

The chapter of my dissertation titled “Loss of PodJ in *Agrobacterium tumefaciens* leads to ectopic polar growth, branching, and reduced cell division” was accepted for publication in the Journal of Bacteriology as of May 2016.

1 AN INTRODUCTION TO POLAR GROWTH AND CELL DIVISION IN *AGROBACTERIUM TUMEFACIENS*

1.1 PLANT TRANSFORMATION BY *A. TUMEFACIENS*

Agrobacterium tumefaciens is a soil dwelling gram-negative alphaproteobacterium pathogen capable of genetically modifying host plant cells. *A. tumefaciens* utilizes a vir-Type 4 Secretion System (*vir*-T4SS) to transfer a single-stranded T-(transfer)-DNA molecule along with protein effectors across the bacterial envelope to the host plant cell, where the T-DNA is targeted to the nucleus and integrated into the host plant chromosome. The T-DNA molecule codes for the production of plant hormones to form the crown gall tumor and opines which serve as a Carbon and Nitrogen source for the bacteria (1).

The *vir*-T4SS is composed of the protein products of 11 genes in the *virB* operon, VirB1-VirB11, and VirD4. These genes for these proteins all reside on the Ti plasmid. Expression of the *vir*-T4SS is induced by phenolic compounds produced during plant wounding (1). During the induction of the virulence apparatus, *A. tumefaciens* inserts the *vir*-T4SS at multiple periodic positions throughout the periphery of the cell (2, 3). Large trans-envelope complexes such as the *vir*-T4SS must pass through the PG layer, a covalently closed mesh located between the inner and outer membranes of Gram-negative cells. The pore size of Gram-negative PG is 2.2 nm, with a diffusion limit of 55 kDa for globular proteins (4). Lytic transglycosylase activity is often required for the assembly of large transenvelope protein complexes such as the *vir*-T4SS, since these complexes are 20 nm wide and larger than the pore size of the PG mesh (5). Indeed, the N-terminus of the VirB1 protein is homologous to known lytic transglycosylases (6), and deletion of *virB1* attenuates DNA transfer via the *vir*-T4SS to levels ≤ 3% of WT (7, 8), suggesting that the VirB1 protein product plays a role in *vir*-T4SS assembly.

1.2 THE GRAM-NEGATIVE BACTERIAL CELL WALL

Though the VirB1 protein is likely involved in PG remodeling to accommodate the *vir*-T4SS, understanding of the biogenesis of the PG mesh is relevant for understanding the assembly of the *vir*-T4SS. I will next review the architecture of the PG mesh in gram-negative bacteria and the enzymes known to be involved in PG synthesis.

In gram-negative organisms, the peptidoglycan cell wall consists of strands of N-acetyl-muramic acid and N-acetyl glucosamine disaccharides, which are oriented in hoops around the circular diameter of the cell, perpendicularly to the long axis of the cell. Each disaccharide precursor is covalently linked to a pentapeptide. When the disaccharides are incorporated into the glycan strands of the peptidoglycan, these pentapeptide stems are processed and cross-linked, resulting in a covalently linked peptidoglycan mesh surrounding the cell membrane (9). As a result, gram-negative peptidoglycan synthesis requires transport of disaccharide-pentapeptide monomers from the cytoplasm to the periplasm, insertion of new disaccharide precursors to the cell wall via

glycosyltransferase activity as well as peptide cross-linking by enzymes with transpeptidase activity (10).

Enzymes fulfilling these PG synthesis activities are known in *Escherichia coli*. The enzymes MurA-G, MraY, MurJ, and DdlA synthesize the PG precursors and covalently link the precursor to the transport lipid undecaprenyl phosphate to form Lipid II on the inner face of the inner membrane. Lipid II is flipped into the periplasmic space by a lipid flippase. Precursors are transferred from Lipid II to nascent PG chains by glycosyltransferases (PBP1A and B). PBP1A and B are also Penicillin-Binding Domain proteins (PBPs). PBPs often have D,D-Transpeptidase activity, forming a peptide bond between neighboring D-amino acids in the peptides of the PG mesh. Thus, PBP1A and B are known as bifunctional PBPs, displaying both glycosyltransferase and transpeptidase activities. Other PBPs exist with D,D-transpeptidase activity (such as PBP3 and PBP2 in *E. coli*), and still other PBPs catalyze miscellaneous transpeptidase activities (10). Cell division also requires amidase activity, present in enzymes such as AmiA, B and C, which removes peptide groups from the glycan strands (11).

Cell wall synthesis generally occurs as part of two growth modes in rod-shaped bacteria: division and elongation. For division, cell wall synthesis must occur at the midcell, resulting in septation. A protein complex called the divisome assembles at the midcell, with periplasmic, inner membrane, and cytoplasmic localizing proteins. The divisome is responsible for septal peptidoglycan synthesis, which drives cell division. The cytoplasmic proteins of the divisome include the tubulin homolog *ftsZ* and the actin-like *ftsA* (12). The *A. tumefaciens* genome encodes homologs of many of the divisome components, including *ftsA* and *ftsZ* (13, 14). In model rod-shaped bacteria such as *E. coli*, the localization of these proteins is predominantly at the midcell for cell division. Localization of cell wall synthesis machinery at the midcell must be sufficiently precise to result in a septation event that divides cell material equally. The cell division proteins FtsZ and FtsA recruit a protein complex including PG synthesis and remodeling enzymes. Additionally, rod-shaped bacteria must elongate sufficiently to produce two fully functional daughter cells (12).

Model rod-shaped gram-negative bacteria such as *E. coli* grow through uniform insertion of new peptidoglycan throughout the sidewall of the rod cell. This new cell wall material synthesis is accomplished by a protein complex called the elongase, which includes cytoplasmic, inner membrane, and periplasmic localizing proteins (15). The actin-like protein MreB associates with inner-membrane proteins including MreC, MreD, and RodZ (10).

1.3 Cell wall synthesis and elongation in the Rhizobiales

The components of the elongase and the dispersed mode of cell envelope synthesis, however, are not universally conserved in rod-shaped bacteria. Synthesis of new cell wall material for elongation is not well understood in members of the alphaproteobacterial order Rhizobiales, such as *A. tumefaciens.* Not only do these organisms lack most homologs of the elongase-specific components (14), they also

appear to synthesize new cell wall material in an entirely different unipolar growth mode (13, 14, 16-18) (Figure 1.1). In the wild-type cell cycle of *A. tumefaciens*, the pole resulting from a division event is a growth pole, and as the cell elongates and approaches division, this growth pole develops into an old pole (16). This growth mode necessitates the development and maintenance of polar asymmetry. *A. tumefaciens* therefore serves as both a model for T4SS assembly and the novel polar growth mechanism.

Polar growth in *A. tumefaciens* relies on spatial and temporal regulation of the machinery involved in the creation of new cell envelope material. The majority of peptidoglycan synthesis must occur at the growth pole. Once the cell has elongated sufficiently, the cell wall synthesis machinery must cease activity at the growth pole and begin activity at the division site. Therefore, polar growth must be negatively regulated at a growth pole in the process of becoming an old pole. Additionally, polar growth must be positively regulated at newly created poles derived from septation. Therefore, studying the relationship between polar growth and cell division represents an opportunity to examine pole identity transitions in bacteria.

Other aspects of cell envelope composition change when a growth pole ceases to grow and cell envelope material is synthesized at the midcell. For instance, FM4-64 labeling of *A. tumefaciens* is strongest at the old pole half of young, short cells, and weakest at the growth pole. FM4-64 labeling is also strongest at both poles of cells nearing division, with a decreased fluorescence at the midcell, where septal cell growth is occurring (13). This indicates that other outer membrane cell envelope properties shift between growth poles and old poles.

The developmental events underlying these changes in cell envelope material are unclear. In particular, the mechanisms of polar growth in *A. tumefaciens*, as well as the process localizing and constraining polar growth, are still not well-defined. Surprisingly, cell division components such as FtsZ and FtsA localize consistently to the growth pole of A. tumefaciens during polar growth, in addition to the proteins' localization at the midcell during cell division (13). Growth pole localization of proteins involved in cell division suggests that these proteins may have been co-opted to organize polar growth in addition to cell division. Polar growth in *A. tumefaciens* also involves cell wall synthesis activities different from those involved in sidewall growth in *E. coli*. Where *E. coli* cross-links new peptidoglycan primarily with the DD-transpeptidase activity of PBPs, *A. tumefaciens* also utilizes L,D-transpeptidases to accomplish peptidoglycan cross-linking (14, 18). Labeling of L-D-transpeptidase peptidoglycan cross-linking activity indicates that L,D-transpeptidase activity is localized to the growth pole and division site in growing *A. tumefaciens* cells. Indeed, a specific L,D-transpeptidase localizes to the growth pole and to the midcell (14).

1.4 Morphological responses to cell division blocks in rod-shaped organisms

Cell growth and cell division are clearly inter-related processes. As will be reviewed, many analogous mutations and treatments have been documented to perturb cell

division in both polar-elongating Rhizobiales and sidewall-elongating rod-shaped bacteria such as *E. coli, Bacillus subtilis,* and *Caulobacter crescentus*. Interestingly, these treatments and mutations generally result in branched and swollen morphologies in the Rhizobiales, and filamentous morphologies in sidewall-growers.

In rod-shaped organisms like *E. coli*, that elongate through dispersed addition of new cell envelope material throughout the sidewall of the rod (15), a block in cell division by overexpression of FtsZ results in a filamentous cell morphology (19). In contrast, overexpression of FtsZ in the polar-growing *Rhizobium meliloti* results in swollen and branched morphologies (20).

Cell division, being one of the most fundamental of living processes, is subjected to extensive regulation. The cell must ensure high fidelity complete replication of its genome as well as faithful partitioning of the two genomes into the two daughter cells (21). In *C. crescentus*, DNA replication is limited to stalked cells. Because of *C. crescentus* cell asymmetry, immediately post-division, the sibling stalked cell immediately restarts DNA replication, while the swarmer cell does not replicate DNA until the swarmer cell transtions to stalked cell (22). The *C. crescentus* CcrM DNA methyltransferase methylates GANTC sites, and CcrM activity is restricted to the predivisional cell. As a result, recently replicated DNA is hemi-methylated. Only fully-methylated DNA is competent for replication. As a result, CcrM functions to control cell-cycle progression (23). Constitutive CcrM expression results in abnormal chromosome number and constitutively fully methylated DNA in *C. crescentus*. Additionally, this perturbation leads to filamentous cells (23), indicating that dysregulation of DNA replication and cell cycle progression also blocks cell division. CcrM is widespread in the alphaproteobacteria (22), including in polar growers such as *R. meliloti* (24) and *A. tumefaciens* (25). Overexpression of CcrM, a treatment expected to block cell division based on results in *C. crescentus*, causes the formation of branched and swollen morphologies in *R. meliloti* and *A. tumefaciens* (24, 25).

Other mutations promoting constitutive CcrM activity result in a block in cell division in *C. crescentus*. The *lon*- mutant in *C. crescentus* phenocopies the CcrM overexpression mutant, indicating that degradation by Lon protease restricts CcrM activity to the predivisional cell (26). The *lon*- mutation in *A. tumefaciens* causes the formation of branched and swollen cell morphologies (27), again supporting the hypothesis that constitutive overexpression of CcrM in *A. tumefaciens* causes a block in cell division and formation of branched morphologies. Interpretation of *lon* mutant data is, however, complicated by the fact that the Lon protease is involved in many essential cell processes (28).

Monitoring of the genome to ensure proper genome replication is not limited to the events in a normal cell cycle. Many bacteria inhibit cell division upon detection of DNA damage via the SOS response. The *lexA* transcriptional repressor is widely conserved in bacteria. LexA cleavage, stimulated by RecA upon DNA damage, relieves negative transcriptional regulation of genes involved in the SOS response (29). In *E. coli*, the SOS

regulon includes *sulA* (30), encoding a protein which prevents assembly of the Z-ring (31). Overexpression of *E. coli* SulA causes cell filamentation (31). Though many organisms express cell division inhibitors as part of the SOS response, these inhibitors are not well-conserved across bacteria and have disparate targets in the cell division apparatus. In *C. crescentus*, SidA is a cell division inhibitor that targets FtsW, the divisome lipid flippase (32). Like SulA, overexpression of SidA results in filamentous cells due to SidA's inhibition of cell division (32). In *B. subtilis*, the protein YneA is similarly SOS-induced and inhibits cell division when overexpressed (33). Mitomycin C, which creates inter-strand DNA cross-links, induces the SOS response and expression of the various cell division inhibitors described here (31-33). Though no SOS-dependent cell division inhibitor has been characterized in *A. tumefaciens* or other polar-growing Rhizobiales, the widespread presence of cell division inhibitors in diverse organisms suggests that a mechanism for halting cell division is universal in the SOS response. In *A. tumefaciens* and other polar growers such as *R. meliloti*, mitomycin C treatment causes the formation of branched morphologies (20, 34). These observations support the model in which a block in cell division in *A. tumefaciens* results in a branching morphology.

Bacterial cell division can also be modulated by the metabolic state of the cell. For instance, *B. subtilis* and *E. coli* cells grown in rich medium are longer than cells grown in poor medium, and cells switched from poor to rich media do not divide until they have reached the larger size appropriate for the new nutrient conditions. In *B. subtilis*, the glucosyltransferase UgtP regulates cell division based on the nutrient status of the cell (35). UgtP utilizes UDP-glucose as a substrate, and catalyzes the attachment of glucose to diacylglycerol for synthesis of lipotechoic acid. In nutrient poor conditions, the cytoplasmic pool of UDP-glucose is low, and UgtP interacts mainly with itself. In high nutrient conditions, UDP-glucose accumulates, and UgtP interacts also with FtsZ, preventing Z-ring assembly. Steady-state UgtP levels are also higher in cells in nutrient-rich conditions (36). In *E. coli*, an unrelated glucosyltransferase, OpgH, senses UDP-glucose levels and inhibits Z-ring assembly accordingly (37). In contrast, the glutamate dehydrogenase GdhZ is involved in regulating Z-ring assembly and constriction in *C. crescentus*. The control of division by GdhZ in this organism may reflect the importance of amino acids as nutrition sources in Nitrogen-limited aquatic environments. Deletion of *gdhZ* results in a division defect in *C. crescentus*; the cell length distribution of *ΔgdhZ* is skewed towards both much longer (ie, filamentous) and much shorter cells in comparison to WT (38). *gdhZ* is well-conserved in bacteria, and its deletion in the polar-growing Rhizobiale *Brucella abortus* results in a division defect, manifesting by the appearance of branched cells (39).

In addition to controlling cell division based on external signals and the readiness of the cell for division, bacteria must control the location of septation within the cell. In *E. coli*, the MinCDE system is involved in placing the Z-ring at the midcell. The MinCD complex serves as an FtsZ inhibitor, and MinE establishes an oscillation of MinC and D from pole to pole. As a result, the concentration of MinCD is lowest at the midcell, and FtsZ can

polymerize there to form the Z-ring (12). Loss of MinE or overexpression of MinCD results in uniform inhibition of FtsZ throughout the cell, causing a block in cell division and the formation of a filamentous morphology (40). In *B. subtilis*, DivIVA is statically localized to poles and recruits MinCD there via MinJ, serving as the topology determinant for preventing FtsZ assembly at the poles. Depletion of DivIVA causes a uniform block in cell division and the cell filamentation phenotype (41, 42). *S. meliloti* possesses *minCDE* homologs, and if these genes function to regulate the localization of the Z-ring as in *E. coli*, a *minE*- strain should display a cell division defect because of uniform inhibition of FtsZ assembly. Indeed, *minE*- cells or cells overexpressing MinCD display a branching phenotype (43). However, deletion of the entire *minCDE* operon in *S. meliloti* does not produce a mutant phenotype (43). Potentially, systems constraining division site localization are redundant in bacteria. As a result, a complete deletion of one system may not impact cell morphology, while interfering with the stoichiometry required for normal function can impact cell morphology.

1.5 POLAR DEVELOPMENT IN THE ALPHAPROTEOBACTERIA

Other alphaproteobacteria possess well-characterized systems for orchestrating polar development. Though Alphaproteobacteria such as *Caulobacter* do not grow through unipolar growth, polar asymmetry and development is a noted feature of their cell cycles. In *Caulobacter*, a non-motile stalked cell elongates, giving rise to a motile swarmer cell, which embarks on a developmental program to become a division-capable stalked cell. The stalk of the stalked cell is a polar organelle located at the old pole opposite of the new pole created from the last division event. The swarmer cell develops flagella and pili specifically at its old pole, and discards these organelles to form a stalk at this pole during its transition to a stalked cell (44).

Regulation of gene expression is critical for cell-cycle progression in *C. crescentus*, and is generally accomplished by two-component signal transduction. In two-component signaling systems, histidine kinases phosphorylate response regulators, which can pass their phosphates to other response regulators via histidine phosphotransferases, or act as transcription factors. CtrA is a key master response regulator of cell cycle gene expression in *C. crescentus*, and CtrA activity is regulated at three levels: proteolysis, transcription, and phosphorylation state. CtrA is proteolyzed in the swarmer-stalked cell transition by ClpXP protease, and lack of CtrA allows chromosome replication to commence during this transition. *ctrA* transcription is controlled by CtrA itself, and is influenced by DNA methylation at the *ctrA* promoter. Activated CtrA positively regulates expression of the CcrM methyltransferase, which methylates the *ctrA* promoter, decreasing CtrA expression (44). Phosphorylated CtrA represses the transcription of *gcrA*, another cell cycle regulator. When CtrA is proteolyzed, GcrA expression is de-repressed. GcrA in turn controls CtrA expression. Oscillating levels of CtrA and GcrA drive the cell cycle through the swarmer and stalked cell developmental stages (45). CtrA is conserved among alphaproteobacteria, though the details of cell cycle regulation vary between different taxa (46).

CtrA phosphorylation is influenced by the histidine kinases DivJ, PleC, CckN, CckO, CckA, and DivL. Establishment of polar asymmetry is accomplished by polar localization of DivJ, PleC, and CckA. The PodJ protein plays a role in localization of PleC, and as a result the development polar organelles such as pili, flagella, and the stalk. The PodJ protein is processed into a short form in a cell-cycle dependent fashion. After division, the short form is localized at the flagellated pole, and the long form accumulates at the pole opposite of the stalked pole as the predivisional cell develops (47, 48). In *S. meliloti,* which also grows through unipolar elongation, *podJ* plays a role in maintenance of normal cell morphology, localization of cell-cycle regulating factors, motility, and composition of the cell envelope (49). Another *Caulobacter* polar localizing protein, PopZ, plays a role in development of the flagellated pole into the stalked pole and in chromosome segregation. The PopZ protein localizes at the flagellated pole after cell division, remains localized at that pole as it develops into a stalked pole, and accumulates at the pole opposite to the stalked pole as the cell approaches division (50-52).

Asymmetric cell division in *C. crescentus* relies on the establishment of asymmetric poles. Moreover, these poles develop over the course of the cell cycle. As a result, there are obvious parallels between *A. tumefaciens* growth pole development and polar asymmetry in *C. crescentus*.

1.6 Connections between polar growth, development, and cell division in *A. tumefaciens*

In this thesis, I present studies on the role of $podJ_{At}$ in polar growth and cell division in *A. tumefaciens*, the relationship between cell morphology and *ftsZ*, and the impact of antibiotics targeting cell wall synthesis on cell morphology. Cells with a $podJ_{At}$ deletion were found to initiate ectopic polar growth and displayed reduced cell division. Expression of an FtsZ point mutant putatively defective in GTP binding and hydrolysis was found to cause morphological deviations from rod-shape, whereas deletion of the shorter midcell-localizing FtsZ2 was not found to impact cell division. Treatment with antibiotics inhibiting PG cross-linking causes the formation of midcell bulges and branched morphologies.

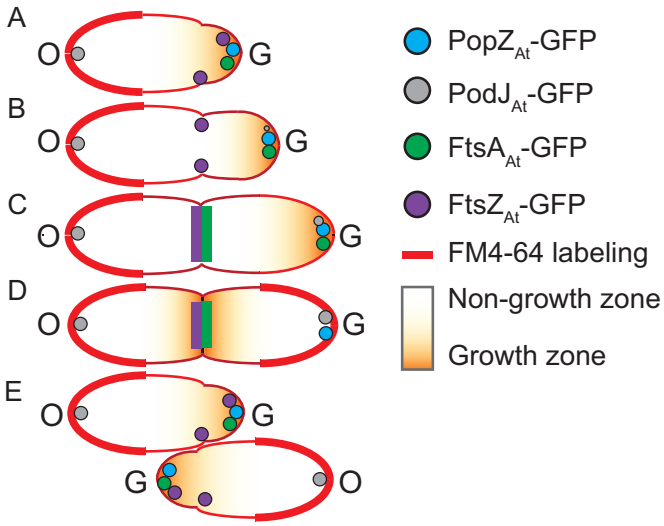

Figure 1.1 Cell growth, division, and localization of marker proteins in *A. tumefaciens.* A) newborn cell, B-C) elongating cell, D) dividing cell, and E) newborn sibling cell stages of the cell cycle. FM4-64 labeling patterns are shown, with thicker red lines indicating areas of increased fluorescence intensity.

2 STANDARD AND UNIQUE MATERIALS, METHODS, AND PROTOCOLS

2.1 STRAINS AND GROWTH CONDITIONS

A. tumefaciens strain C58 containing pTiC58 (53) was transformed with the relevant plasmids. Cells were inoculated into LB media overnights at 28° C. Cells were diluted to OD_{600} = 0.1 in LB media at 28° C and grown for four hours or AB media pH 5.5 at 19° C and grown for five hours (2). For time-lapse experiments, overnight cultures were diluted to 10^8 cells/ml and grown for 4-5 hours before imaging. Lactose-inducible expression was achieved by adding 2.5 mM IPTG (isopropyl-β-d-thiogalactopyranoside) to cultures.

2.2 MOLECULAR CLONING AND STRAIN CONSTRUCTION

Standard molecular cloning techniques were used to construct strains (54). The *ΔpodJ*$_{At}$ and *ΔftsZ2* strains were constructed by transforming C58 with pJZ237 and pJAF044, selecting for a single crossover into the genome by growing on carbenicillin, then selecting for a second recombination by growth on sucrose. pJZ237 (Table 5.1) is derived from a vector created by cloning the *B. subtilis sacB* gene conferring sucrose sensitivity (55) into a SacI site in the Stratagene pBlusescript II SK vector, which cannot replicate in *A. tumefaciens*. pJZ178 was further created by cloning *kan*^{R} into the SalI and SpeI sites of pJZ237. The deletions of *podJ*$_{At}$ and *ftsZ2* were verified by PCR and sequencing.

2.3 FLUORESCENCE MICROSCOPY

Cells were grown in LB overnight, diluted in LB with IPTG, and grown for four hours. Slides with agarose pads (1% agarose in PBS pH 7) were prepared. Cells were resuspended in FM4-64 for 5 minutes, applied to agarose pads, covered with a coverslip, and imaged on the Deltavision Microsope.

2.4 SCANNING ELECTRON MICROSCOPY

Cells were fixed in 2% glutaraldehyde in 0.1 M sodium cacodylate buffer, rinsed with sodium cacodylate buffer, post-fixed in 1% osmium tetroxide in sodium cacodylate buffer, dehydrated to 100% ethanol, critical point dried, mounted on gold stubs, and imaged using a Hitachi S-5000 scanning electron microscope.

2.5 CELL LABELING

Approximately 9 x 10^8 cells were fixed in ice-cold methanol for 10 minutes at -20 C in 5 μg/mL FM4-64FX (Life Technologies) to stain cell membranes. 2-3 μL of cells were pipetted onto poly-L-Lysine coated coverslips and air-dried. Coverslips were washed 3 times with PBS pH 7, and 1 μg/mL 4',6-diamidino-2-phenylindole (DAPI) was added to cells. Texas Red Succinimidyl Ester (TRSE) labeling was performed as described previously (14).

3 LOSS OF PODJ IN *AGROBACTERIUM TUMEFACIENS* LEADS TO ECTOPIC POLAR GROWTH, BRANCHING, AND REDUCED CELL DIVISION

3.1 INTRODUCTION

Cell wall synthesis generally occurs in two modes in well-studied Gram-negative rod-shaped bacteria such as *Escherichia coli*. For division, cell wall peptidoglycan synthesis occurs at the mid-cell, resulting in septation. A protein complex called the divisome is responsible for septal peptidoglycan synthesis. The tubulin homolog FtsZ and the actin-like FtsA are essential for divisome structure and function. In model rod-shaped bacteria the localization of these proteins at the mid-cell ensures equal division into two daughter cells (15). Additionally, rod-shaped bacteria must elongate prior to the subsequent division. This second mode of cell wall synthesis involves uniform insertion of new peptidoglycan laterally throughout the sidewall of the rod and is accomplished by a protein complex called the elongase (56-58).

Members of the α-proteobacterial order Rhizobiales, such as *Agrobacterium tumefaciens,* undergo cell division at the mid-cell and encode most of the known divisome components (14). However, these bacteria produce new peptidoglycan material for elongation in a remarkably different manner involving a single pole of the bacterial cell (17). Peptidoglycan synthesis at the growth pole occurs by a mechanism that maintains rod shape and is similar to the growth mode of *Streptomyces* and *Mycobacteria* species (59-62). Once the *Agrobacterium* cell has elongated sufficiently, cell wall synthesis machinery ceases activity at the growth pole and begins activity at the division site (14, 18). New growth poles in daughter cells arise at the poles created by division (13, 18). Finally these organisms lack homologs of most of the elongase components, found in well-studied bacteria such as *Escherichia coli* or *Caulobacter crescentus* (14).

Unipolar growth in *A. tumefaciens* necessitates the development and maintenance of polar asymmetry by spatial and temporal regulation of the machinery involved in the creation of new cell envelope material. Remarkably, *A. tumefaciens* cell division proteins are possibly involved in polar growth, as hallmark cell division proteins such as FtsA and FtsZ localize to the growth pole during polar growth, and subsequently localize to the mid-cell during division (13, 14, 63). As the cell approaches division, elongation at the growth pole stops and this pole transitions to an old pole (13, 14, 18). Therefore, polar growth must be negatively regulated during the switch to becoming an old pole.

To further understand *A. tumefaciens* polar growth and to identify molecular players in pole identity, we are studying the localization patterns of proteins known to play roles in polar development in other α-proteobacteria (52). Though some α-proteobacteria such as *C. crescentus* do not grow through unipolar growth, polar asymmetry and

development is a noted feature of their cell cycles. Several *C. crescentus* gene products are asymmetrically localized in a cell-cycle dependent fashion to affect these developmental processes. One *C. crescentus* polar localizing protein, $PopZ_{Cc}$, is required for development of the flagellated pole into the stalked pole and for chromosome segregation (52, 64-66). The product of another gene, $PodJ_{Cc}$ functions in development of polar organelles such as pili, flagella, and the adhesive holdfast (47), and is involved in the polar localization of cell-cycle regulators such as PleC (47, 48). In *Sinorhizobium meliloti* (RM1021), which grows through unipolar elongation like *A. tumefaciens* (18), deletion of *S. meliloti* (RM1021)-specific *podJ1* alters cell morphology, flagellar motility, cell envelope composition, and localization of cell-cycle regulating factors such as DivK (49).

Putative homologs of $PodJ_{Cc}$ and $PopZ_{Cc}$ were recently characterized in *A. tumefaciens* (67). While $PopZ_{At}$ localizes exclusively to growing poles GFP-$PodJ_{At}$ localizes predominantly to the old pole, and accumulates at the growth pole late in the cell cycle as the growth pole transitions into an old pole (67); thus, we suggested that $PodJ_{At}$ may determine old pole identity in *A. tumefaciens*. To further test the role of *A. tumefaciens* specific $PodJ_{At}$ in orchestrating polar development, we created a $podJ_{At}$ deletion. Indeed, deletion of this gene resulted in ectopic growth poles and cell division defects that dramatically altered cell morphology. Notably, $PopZ_{At}$ localized to ectopic poles in the $podJ_{At}$ deletion and the cell division proteins FtsA and FtsZ localized to division sites that failed to septate. Together, these data suggest $PodJ_{At}$ is a critical factor in normal polar growth and its absence impacts cell division.

3.2 MATERIALS AND METHODS

3.2.1.1 Strains and cell growth conditions

Strains used in this study are listed in .

Table 3.1 Strains and plasmids used in this study

Strains	Relevant genotype	Source
XL1 Blue	*E. coli* cloning strain, *endA1 gyrA96*(nal^R) thi-1 *recA1 relA1* lac glnV44 F'[::Tn10 *proAB+ lacIq* Δ(*lacZ*)M15] hsdR17(rK-mK+), Tet^R.	Lab stock
C58	wild-type *A. tumefaciens* strain C58	Lab stock
A164	C58, $\Delta podJ_{At}$, using pJZ237	This work
NT1REB	Rm^R Em^R pTi$^-$ mot$^-$ *ΔflaABC* (bald strain)	(68)
Plasmids	**Relevant genes and construction information**	**Source**
pSRK-Km	Broad host-range, lac inducible, Kan^R	(69)
pSRK-Gm	Broad host-range, lac inducible, Gent^R	(69)
pBluescript II SK	Phagemid, Carb^R	Stratagene

pJZ156	pBSKII+ with *sacB*, Carb^R	This work
pJZ207	pSRK-Km with *ftsZ-GFP*, lac-inducible, Kan^R	(13)
pJZ208	pSRK-Km with *ftsA-GFP*, lac-inducible, Kan^R	(13)
pJZ232	pSRK-Gm with *gfp-podJ$_{At}$*, lac-inducible, Gent^R	(67)
pJZ237	pJZ156 with 1kb sequences homologous to C58 genomic DNA flanking Atu0499 (*podJ$_{At}$*) and Atu0500, Carb^R	This work
pJZ255	pSRK-Gm with *podJ$_{At}$*, lac-inducible, Gent^R	This work
pRG001	pSRK-Gm with *popZ$_{At}$-gfp*, lac-inducible, Gent^R	(67)

3.2.1.2 Flagellar motility assay

Flagellar motility assays were performed on semisolid LB media with 0.3% agar plates. Small colonies grown on regular LB agar plates were picked with sterile thin P200 pipette tips. The pipette tips were submerged into the semisolid agar and imaged after two days of incubation at 28 C.

3.2.1.3 Spot titer growth assay

Cells were grown overnight in LB at 28 C, diluted to 10^8 cells/ml and grown for 4-5 hours in the media used for growth characterization. Cell suspensions were then diluted in a series of tenfold dilutions in the same growth medium. 10 μL of cell suspension for each dilution was spotted on plates in the indicated area. Plates were incubated for two days at 28 C and imaged.

3.2.1.4 Time-lapse microscopy

B04A microfluidic plates were used with the CellASIC ONIX microfluidic system. Plates were flushed with LB with appropriate antibiotics and inducer for 30 minutes at 4 psi. Cells (100 μL at 3 x 10^9 cells/mL) were loaded into the microfluidics chamber from a suspension at 3x10^9 cells/mL and perfused with LB with appropriate antibiotics and inducer. Cells were imaged in a chamber with a ceiling height of 0.9 to 1.1 um for 3-4 hours. Cells were then imaged on an Applied Precision Deltavision deconvolution fluorescence microscope. Images were processed using Fiji software.

3.3 RESULTS

We recently characterized the localization of *A. tumefaciens* wild type (WT) GFP-PodJ$_{At}$ and PopZ$_{At}$-GFP. While PopZ$_{At}$ remains a growth pole specific marker throughout the cell cycle, GFP-PodJ$_{At}$ localizes to the old pole and then also to the growth pole during the later stages of polar elongation, potentially marking the transition of the growth pole into an old pole just prior to cell division (67). The localization patterns of GFP-PodJ$_{At}$ and PopZ$_{At}$-GFP as well as the cell division proteins FtsA-GFP and FtsZ-GFP are summarized in Figure 1.1. To provide further insight into the requirement for the dynamic localization of GFP-PodJ$_{At}$ we monitored cell cycle progression and the localization of polar development proteins in a *podJ$_{At}$* deletion strain (*ΔpodJ$_{At}$*).

podJ$_{At}$ (Atu0499) is located in a genomic context more similar to *podJ*$_{Sm}$ of *S. meliloti* strain SM11 than *podJ*$_{Cc}$ of *C. crescentus* (Figure 3.1) as might be expected for two members of the Rhizobiales. *ΔpodJ*$_{At}$ was created through allelic exchange resulting in a markerless deletion of the Atu0499 open reading frame and the short hypothetical Atu0500 open reading frame that overlaps the 5' end of Atu0499. Transcription of Atu0500, however, was not detected in microarray data, indicating it is not likely expressed (70). Deletion of *podJ*$_{At}$ was verified by PCR amplification of the Atu0499 locus and flanking regions from genomic DNA and sequencing of the PCR product.

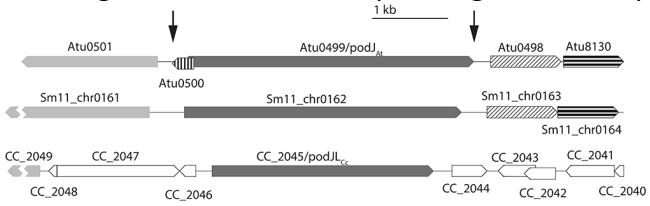

Figure 3.1 *podJ* genomic contexts in *A. tumefaciens*, *S. meliloti*, and *C. crescentus*. Atu numbers refer to *A. tumefaciens* strain C58 locus tags, Sm11_chr numbers refer to *S. meliloti* strain SM11 locus tags, and CC_ numbers refer to *C. crescentus* CB15N locus tags. ORFS that are similarly colored or textured are reciprocal best BLAST hits. ORFS that are white are not homologous to any other ORF shown. Breaks in *S. meliloti* and *C. crescentus* ORFs reflect ORFs that extend beyond the area shown. *ΔpodJ*$_{At}$ was created using allelic exchange to remove both *podJ*$_{At}$ and the small overlapping reading frame Atu0500 in the region between the arrows.

3.3.1.1 Deletion of *podJ*$_{At}$ results in major growth abnormalities

Deletion of *podJ*$_{At}$ causes morphological aberrations compared to WT *A. tumefaciens*. *ΔpodJ*$_{At}$ cells stained with the membrane dye FM4-64 (Figure 3.2 A-B) are elongated, often with multiple constrictions. In WT cells FM4-64 predominantly stains the old non-growing poles (12) as summarized in Figure 1.1. Notably, many *ΔpodJ*$_{At}$ cells are branched or swollen. Bent cells and small spherical *ΔpodJ*$_{At}$ cells are also observed. The frequencies of morphological deviations from rod shape observed in *ΔpodJ*$_{At}$ cells compared to WT cells are summarized in . In scanning electron microscopy (SEM) images of *ΔpodJ*$_{At}$ cells, constrictions are more numerous than in lower resolution light micrographs and cells with multiple branches are also better resolved (Figure 3.2 C-D). A gallery of SEM images of *ΔpodJ*$_{At}$ cells (Figure 3.4 A-F) shows additional examples of branched and multiply constricted cells as well as cells with tapered poles.

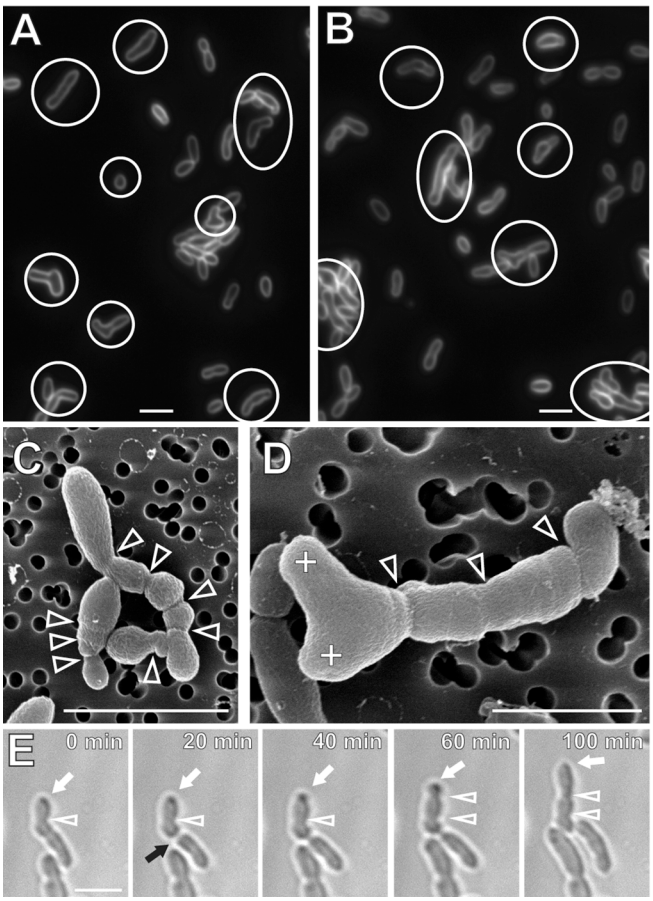

Figure 3.2 *ΔpodJ$_{At}$* cells are elongated, branched, multiply constricted, and swollen, and show ectopic polar growth. A) and B) FM4-64 labeled *ΔpodJ$_{At}$* cells. Cells with morphological deviation from rod shape, such as cells with multiple constrictions, branched cells, swollen cells, and bent cells, are indicated with ellipses. C) and D) SEM images of *ΔpodJ$_{At}$* cells displaying deviations from rod-shape morphology including elongated cells, branched cells, and cells with multiple constrictions. Arrowheads denote cell constrictions (variations in cell width). + signs indicate branch tips. E) Time lapse images of *ΔpodJ$_{At}$* cells undergoing polar growth (white arrow) and a division event (black arrow). White arrowheads denote cell constrictions.

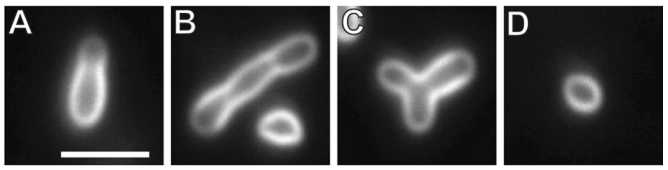

	WT	Δ*podJ*$_{At}$	Δ*podJ*$_{At}$+ GFP-PodJ$_{At}$	Δ*podJ*$_{At}$+ PodJ$_{At}$
A: Rod-shaped	96%	60%	87%	93%
B: Multiple constriction/ bent	4%	29%	7%	4%
C: Branched/ swollen	0%	8%	5%	2%
D: Minicell	0%	3%	1%	1%

Figure 3.3 Frequency of morphological abnormalities in *ΔpodJ*$_{At}$ cells. Percentages of WT cells (n=283), *ΔpodJ*$_{At}$ cells (n=262), *ΔpodJ*$_{At}$ cells expressing GFP-PodJ$_{At}$ (n=340) and *ΔpodJ*$_{At}$ cells expressing PodJ$_{At}$ (n=247) displaying different morphologies are shown below representative images.

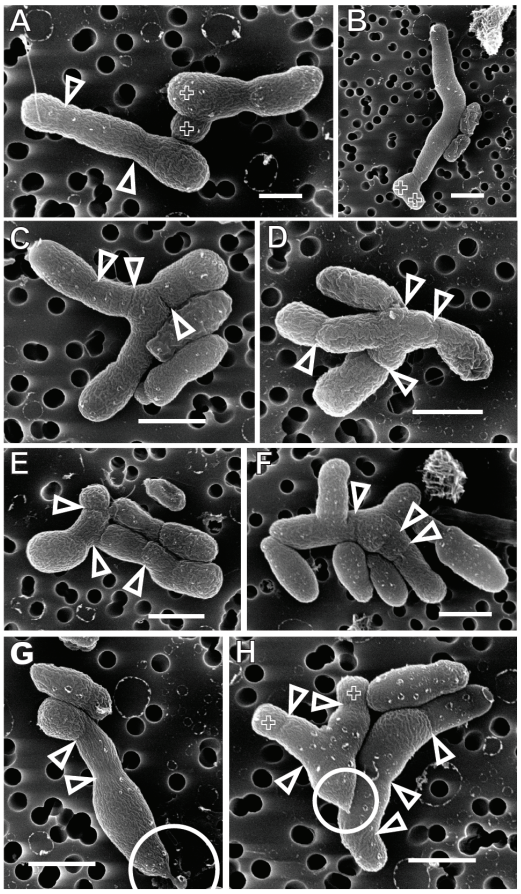

Figure 3.4 Gallery of scanning electron microscope images of *ΔpodJ*$_{At}$ cells. A) and B) show elongated cells with branches and constrictions. C)-F) show branched cells with multiple constrictions. G) and H) show cells with tapered poles, branches, and multiple constrictions. Arrowheads denote constrictions, + signs denote branch tips, and circles denote tapered poles. Scale bars, 3 μm.

We then used time-lapse light microscopy to follow the morphological deviations from rod-shape that occur during the *ΔpodJ*$_{At}$ cell cycle. Identification of growth poles in time-lapse images of *A. tumefaciens* is based on cell morphology. In WT *A. tumefaciens*, the parent cell compartment, with an old, non-growing pole at its end, is consistently larger in width than the new cell compartment, with a growing pole at its end. As the cell approaches division, the growth pole widens to attain the same width as the old, non-growing pole. The difference in widths between mother and daughter cell compartments can be used to distinguish the growing daughter cell end of the cell from the non-growing end (14, 18).

Identification of growth poles based on the width of cell compartments in time-lapse microscopy is also supported by pulse-chase labeling of cell envelope material in *ΔpodJ*$_{At}$ and WT (Figure 3.5). Texas Red Succinimidyl Ester (TRSE) labels outer membrane proteins in *A. tumefaciens* (14, 18). In a chase period after cell labeling, new unlabeled cell envelope material is added to growing *ΔpodJ*$_{At}$ cells (Figure 3.5 A, 30 to 50 min, Figure 3.5 B, 30 to 40 min, and WT cells, Figure 3.5 C, 20 to 40 min). All unlabeled new poles are smaller in width than the labeled, non-growing poles.

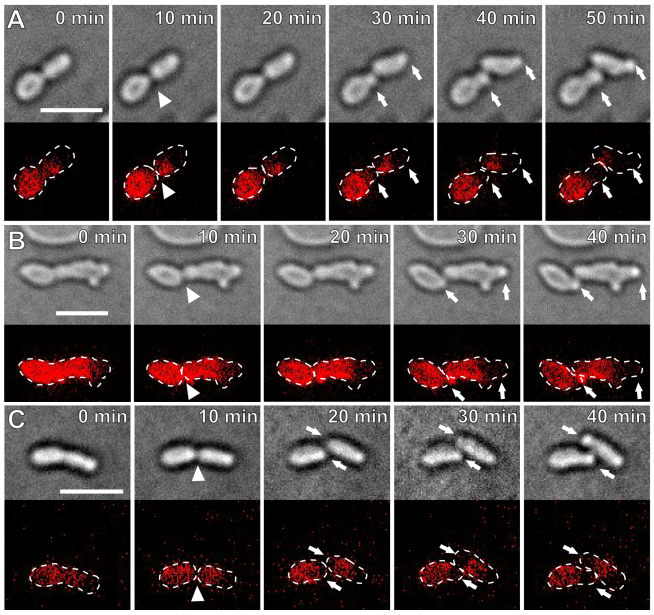

Figure 3.5 Pulse-chase labeling indicates growth abnormalities and that growing poles are smaller in diameter than non-growing poles in *ΔpodJ*$_{At}$. Live-cell imaging of *ΔpodJ*$_{At}$ cells pulse-chase labeled with TRSE. Unlabeled areas indicate sites of new cell growth during chase period. A) After division (white arrowhead) the cell on the right continues to grow from the growth pole (white arrow). B) After division (white arrowhead), the cell on the right continues to grow from the growth pole (white arrow) and develops a branch morphology via ectopic polar growth. C) A WT cell undergoing normal polar growth (white arrows) from poles derived from a division event (white arrowhead). Top: brightfield images. Bottom: red fluorescence images. Scale bar, 3 µm.

Some *ΔpodJ*$_{At}$ cells continue to grow from the pole opposite the division site, which normally would be the old non-growing pole in WT cells (Figure 3.2 E, Figure 3.5 A, 30 to 50 min, cell on the right, and Figure 3.5 B, 30 to 40 min, cell on the right). In contrast WT cells grow from poles derived from a division event (Figure 3.5 C, 20 to 40 min, and

schematic of WT growth, Figure 1.1). Ectopic polar growth (Figure 3.2 E, white arrow) continues for at least 80 minutes. This cell also develops two constrictions (Figure 3.2 E, arrowheads) that normally indicate the site(s) of septum formation; however, no septum formation was observed in this *ΔpodJ*$_{At}$ cell.

Though 60% of *ΔpodJ*$_{At}$ cells appear morphologically normal in static images (Figure 3.3), time-lapse imaging suggests that many of these cells develop altered morphologies during the course of one or two cell cycles. Figure 3.2 E shows an example of a cell that begins by apparently normal polar growth and division, but then give rise to sibling cells with ectopic growth poles and defects in morphology. Thus, the development of *ΔpodJ*$_{At}$ morphological phenotypes is a stochastic process.

As time-lapse microscopy better documents the *ΔpodJ*$_{At}$ phenotype, we next quantified the patterns of growth during time lapse imaging of 151 *ΔpodJ*$_{At}$ cells and 148 WT cells during the cell cycle (Table 3.2). Division events produced two sibling cells displaying a normal pattern of polar growth in 100% of WT cells and in only 53% of *ΔpodJ*$_{At}$ cells. In *ΔpodJ*$_{At}$ 37% of cells produced one cell with an ectopic growth pole, 3% gave rise to one normal-growing cell and one non-growing cell, and 7% gave rise to one ectopic polar-growing cell and one non-growing cell.

Table 3.2 Percentages of WT, *ΔpodJ*$_{At}$, and *ΔpodJ*$_{At}$ + PodJ$_{At}$ division events producing normal polar growing, ectopic polar growing, and non-growing cells. Numbered schematics representing types of division events are shown, with the pre-divisional cell above and resulting sibling cells below. G, normal growth poles. E, ectopic growth poles. N, non-growing poles. Filled cells represent non-growing cells. These data are derived from time-lapse imaging of individual cells (n).

Types of division events	**WT** **(n=148)**	***ΔpodJ*$_{At}$** **(n=151)**	***ΔpodJ*$_{At}$ + PodJ$_{At}$** **(n=142)**
1) Producing two normal polar-growing cells	100%	53%	95%
2) Producing one normal polar-growing cell and one ectopic polar-growing cell	0%	37%	3%
3) Producing one normal polar-growing cell and one non-growing cell	**0%**	**3%**	**1%**
4) Producing one ectopic polar-growing cell and one non-growing cell	0%	7%	1%
1)  2) 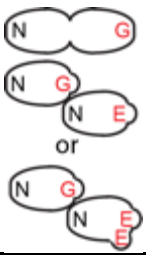 3) 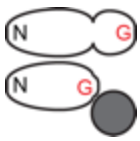 4) 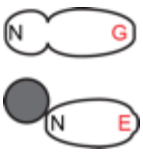			

The growth rate of *ΔpodJ$_{At}$* as measured by the optical density of a culture at 600nm (OD_{600}) in liquid medium was not different from WT (Figure 3.6). However, the mean colony forming units (CFU) mL^{-1} OD_{600}^{-1} was 1.24 x 10^9 (n=6) for WT, and only 1.09 x 10^9 (n=6) for *ΔpodJ$_{At}$*. A two-tailed t-test gave a p value of 0.0193, indicating a significant difference in colony forming ability between the two strains, potentially due to lower viability of larger or very short *ΔpodJ$_{At}$* cells (see below). Alternatively, the longer and branched cells in *ΔpodJ$_{At}$* may increase their optical density (compared to WT) while yielding lower CFUs. Thus, in spite of morphological abnormalities, *ΔpodJ$_{At}$* is capable of growth and division.

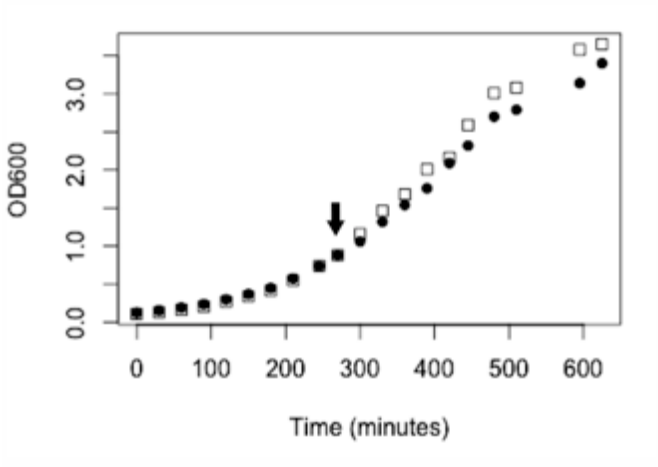

Figure 3.6 Growth of *ΔpodJ$_{At}$* cells is similar to wild type. OD600 growth curve for C58 (□) and *ΔpodJ$_{At}$* (•). Arrow indicates time when CFU/mL were determined (see text).

3.3.1.2 GFP-PodJ$_{At}$ expression partially complements, and PodJ$_{At}$ expression fully complements, *ΔpodJ$_{At}$* growth abnormalities

We tested whether limited expression of GFP-PodJ$_{At}$ or unfused PodJ$_{At}$ under control of a tightly regulated *lac* promoter on a low-copy plasmid (69) could complement *ΔpodJ$_{At}$*. A large fraction of *ΔpodJ$_{At}$* cells expressing GFP-PodJ$_{At}$ or PodJ$_{At}$ (not fused to GFP) displayed normal rod- shaped morphology (87% and 93 % respectively), compared to *ΔpodJ$_{At}$* (60%) (Figure 3.3). We also monitored 142 *ΔpodJ$_{At}$* cells expressing PodJ$_{At}$ by time-lapse microscopy and found 97% of the division events were normal (Table 3.2). It is notable that PodJ$_{At}$ can still function when fused to GFP. Figure 3.7 exemplifies a cell displaying one growing pole and one non-growing pole (0 to 20 min). Then from 20 to 40 min the cell divides, and from 60 to 100 min, the two daughter cells grow from the poles created by the cell division event just as in WT (13, 18). GFP-PodJ$_{At}$ localized predominantly in larger foci at old poles and to smaller foci in new poles just prior to division (as these poles transition to old poles) as observed in WT (67).

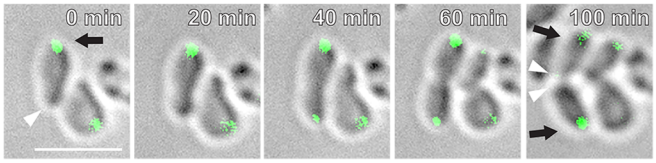

Figure 3.7 Complementation of *ΔpodJ$_{At}$* with GFP-PodJ$_{At}$ restores cell morphology and dynamic polar localization of GFP-PodJ$_{At}$. In the early stages of the cell cycle (0-20 min) GFP-PodJ$_{At}$ localizes as a large focus at the old pole (black arrow). Later on in the cell cycle (40-60 min) GFP-PodJ$_{At}$ localizes also at a smaller focus at the new pole (see white arrowheads at 0 and 100 min). Post division GFP-PodJ$_{At}$ localizes as large foci at old poles (100 min, black arrows). Scale bars, 3 µm.

3.3.1.3 PopZ$_{At}$ localizes to ectopic poles in *ΔpodJ$_{At}$*

During WT septation in *A. tumefaciens* PopZ$_{At}$-GFP disappears from the growth pole of the parent cell and is observed at the growth poles of the sibling cells immediately after completion of cell division (21) (Figure 1.1). However, in *ΔpodJ$_{At}$* cells PopZ$_{At}$-GFP often does not leave the growth pole either just before or after septation (Figure 3.8 A, t=0 to t=60 min, white arrow), and this pole continues to grow ectopically (Figure 3.8 A, t = 80 to 100 min). We monitored 84 dividing *ΔpodJ$_{At}$* cells by time-lapse microscopy and found that in 35 of the dividing cells (42% of total), PopZ$_{At}$-GFP fails to relocalize from the growth pole after division. In contrast, in all 41 WT dividing cells monitored by time-lapse microscopy, PopZ$_{At}$-GFP relocalizes to the poles derived from the division site in both sibling cells.

Table 3.2 documents that often only one of the two *ΔpodJ$_{At}$* sibling cells grows post cell division. We tested whether PopZ$_{At}$-GFP localization can distinguish growing from non-growing *ΔpodJ$_{At}$* sibling cells. Indeed, A shows PopZ$_{At}$-GFP fluorescence appears at the site of division in the lower sibling cell that exhibits polar growth. Notably there is no growth from the division site, and no PopZ$_{At}$-GFP fluorescence, in the upper sibling cell likely because PopZ did not leave the growth pole.

PopZ$_{At}$-GFP also localizes to multiple ectopic growth poles in different *ΔpodJ$_{At}$* cells. In one cell (Figure 3.8 B) both the growing tip and the PopZ$_{At}$–GFP focus start to broaden at 20 min. Between 40 and 80 min, the growth pole as well as the PopZ$_{At}$-GFP focus split to form two growth poles each with a PopZ$_{At}$–GFP focus. In another cell PopZ$_{At}$-GFP localizes to the existing growth pole as well as the ectopic growth pole emerging from a point along the sidewall of the cell (Figure 3.8 C, 10 min to 40 min, white arrow). These data together support our previous findings that PopZ$_{At}$ identifies the growth pole (21) and further suggest that PopZ$_{At}$ also identifies sites of ectopic growth either at existing growth poles or *de novo* from a sidewall. Branched cells (Figure 3.2 D, F, and) may reflect the underlying ectopic localization of PopZ$_{At}$ to these sites.

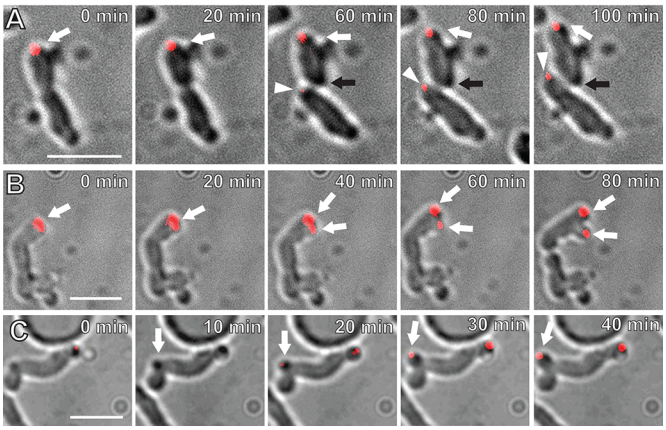

Figure 3.8 PopZ$_{At}$-GFP localizes to ectopic growth poles in *ΔpodJ$_{At}$*. A) The *ΔpodJ$_{At}$* cell on the top displays a PopZ$_{At}$-GFP focus (red) at a growing pole (white arrow) that continues to grow post division. The black arrow indicates a pole produced by division (60 min) that should normally be a growth pole, but it does not grow and does not label with PopZ$_{At}$-GFP. In contrast the lower sibling cell grows from the site of division as in WT (white arrowhead) and this new growth pole does label with PopZ$_{At}$-GFP. B) *ΔpodJ$_{At}$* cell displaying splitting of the growth pole and producing two PopZ$_{At}$-GFP foci (white arrows). C) *ΔpodJ$_{At}$* cell with PopZ$_{At}$-GFP focus at a growth pole emerging from a convex point along the sidewall of the cell (white arrow). Scale bars, 3 µm.

3.3.1.4 *ΔpodJ$_{At}$* is defective in the localization and function of cell division proteins

FtsA-GFP and FtsZ-GFP localize to the growth pole in addition to the Z-ring in WT *A. tumefaciens* (13). In *ΔpodJ$_{At}$*, FtsA-GFP localization patterns are more heterogeneous than in WT cells. Aside from the unipolar, unipolar and midcell, and midcell localization patterns (Figure 3.9 A-C) seen in WT, in *ΔpodJ$_{At}$* FtsA-GFP displays bipolar (Figure 3.9 F), polar plus peripheral foci (Figure 3.9 G), polar cluster localization (Figure 3.9 H), midcell plus bipolar, (Figure 3.9 D) and multiple Z-ring localization (Figure 3.9 E). The percentage of *ΔpodJ$_{At}$* cells displaying some form of midcell FtsA-GFP localization, ~42% (Figure 3.9 B-E), was higher than the percentage of WT cells that had FtsA-GFP midcell localization, 22% (see Figure 2C in (13)). Additionally, the percentage of *ΔpodJ$_{At}$* cells displaying WT polar FtsA-GFP (Figure 3.9 A) localization without midcell localization, 36 %, was significantly lower than the percentage of WT cells with only polar FtsA-GFP localization, 78% (13).

The lengths of *ΔpodJ$_{At}$* cells displaying different types of FtsA-GFP localization (Figure 3.9 I) were compared to the median lengths of WT cells displaying different FtsA-GFP localization patterns determined previously (13) and are summarized in Table 3.3. In all cases, whether *ΔpodJ$_{At}$* cells displayed the WT FtsA-GFP localizations (polar, polar + midcell, and midcell) or aberrant FtsA-GFP localization patterns specific to *ΔpodJ$_{At}$*, the cell length distributions tended towards longer *ΔpodJ$_{At}$* cells than WT cells.

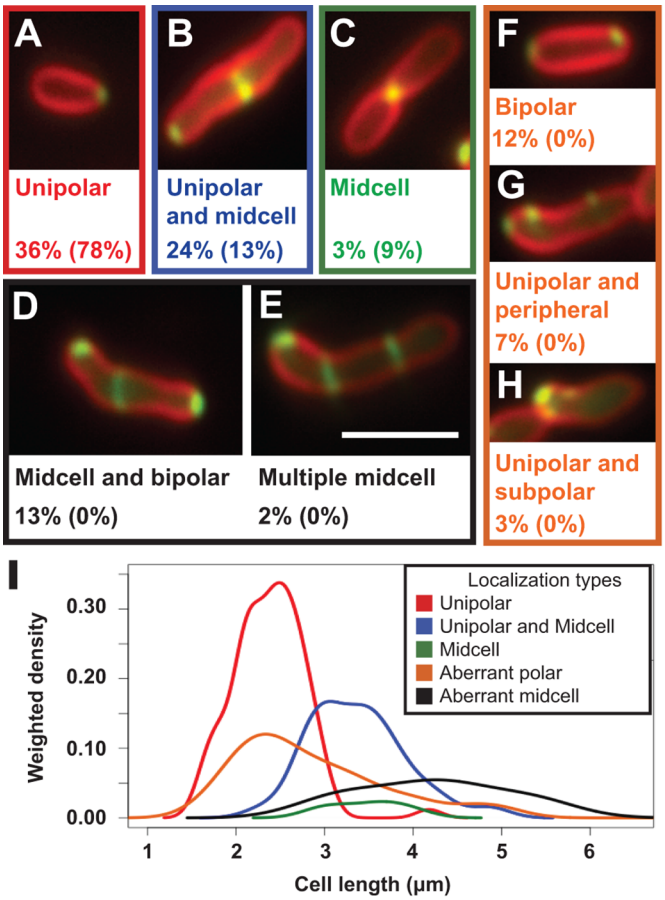

Figure 3.9 FtsA-GFP localizes in polar foci, lateral foci, and rings in elongated *ΔpodJ$_{At}$* cells. *ΔpodJ$_{At}$* cells expressing FtsA-GFP stained with FM4-64 display FtsA-GFP patterns seen in WT cells: unipolar (A), unipolar and midcell (B), and midcell (C) localizations. *ΔpodJ$_{At}$* cells also display localization patterns of FtsA-GFP not observed in WT cells: bipolar and midcell (D), multiple rings (E), bipolar (F), polar and lateral foci (G), and polar clusters (H). The percentages of *ΔpodJ$_{At}$* cells (out of 234 cells total) showing these localization types are shown under representative images, and the percentages of WT cells showing these localization types are shown in parentheses and are from (13). Scale bar, 3 μm. (I) Gaussian kernel density estimates of the distribution of cell lengths of *ΔpodJ$_{At}$* cells with different FtsA-GFP localization patterns. Density estimates were weighted by the proportion of cells displaying the different localization types so that the height of the peaks corresponds to the proportion of cells displaying each localization pattern. Colors of density curves correspond to color outlines of representative images of each localization pattern in (A-H).

Table 3.3 Median cell lengths of WT and *ΔpodJAt* cells displaying the specified FtsA-GFP localization. Values for WT are from Zupan *et al.* (13).

		Unipolar	Unipolar + midcell	Midcell	Aberrant polar	Aberrant midcell
WT	Median cell length (μm)	1.9	2.7	3.2	NA	NA
	Percentage of cells	78	13	9	NA	NA
ΔpodJ$_{At}$	Median cell length (μm)	2.4	3.3	3.5	2.7	4.3
	Percentage of cells	36	24	3	22	15

Localization patterns of FtsZ-GFP in *ΔpodJ*$_{At}$ cells also were compared to previously published localization frequencies of FtsZ-GFP during different stages of the cell cycle in WT cells (13). *ΔpodJ*$_{At}$ displayed a higher percentage of cells with uncontracted Z-rings (Figure 3.10 G) or contracted Z-rings (Figure 3.10 H) (51% total) versus WT (6 % total), and lower percentages of cells with unipolar (10 %) or subpolar (9 %) FtsZ-GFP localizations (19% total) versus WT (57% total) (Figure 3.10). FtsZ-GFP localized in multiple Z-rings in 1% of *ΔpodJ*$_{At}$ cells (Figure 3.10 I). In *ΔpodJ*$_{At}$, FtsZ-GFP localizes in persistent Z-rings that do not result in division and persist for at least 120 min (Figure 3.11, white arrowhead); additionally this cell produces a second Z-ring between 120 minutes to 140 minutes. Finally Z-ring placement can be abnormal; at 60 min there is a small focus at the top of the cell that becomes a Z-ring (Figure 3.11, t= 60 to 100 min) that pinches off a very small spherical "cell" at 120 min.

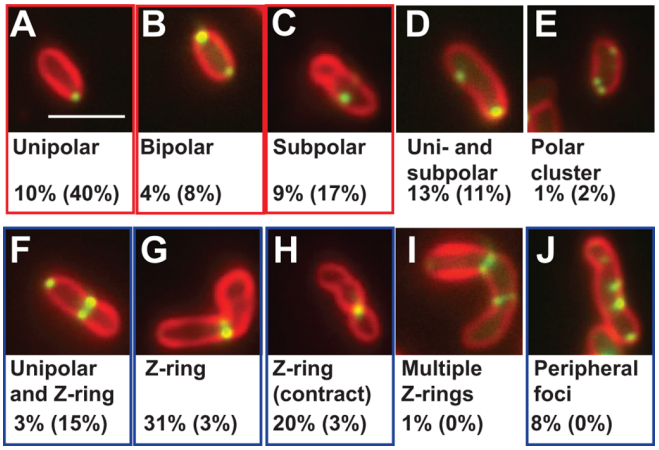

Figure 3.10 FtsZ-GFP localization in *ΔpodJ*$_{At}$. FtsZ-GFP (green) localizes in A) unipolar, B) bipolar, C) subpolar, D) unipolar and subpolar, E) polar cluster, F) unipolar and Z-ring, F) Z-ring, G) contracting Z-ring, H) multiple Z-rings, and I) multiple sidewall foci in *ΔpodJ*$_{At}$. Percentages of *ΔpodJ*$_{At}$ cells (n=252) and WT (13) cells (in parentheses) showing different FtsZ-GFP localizations are shown beneath representative images. Localizations seen in notably higher percentages of WT cells than *ΔpodJ*$_{At}$ cells are highlighted by red rectangles, and localizations seen in notably higher percentages of *ΔpodJ*$_{At}$ cells than WT cells are highlighted by blue rectangles. Scale bar, 3 µm.

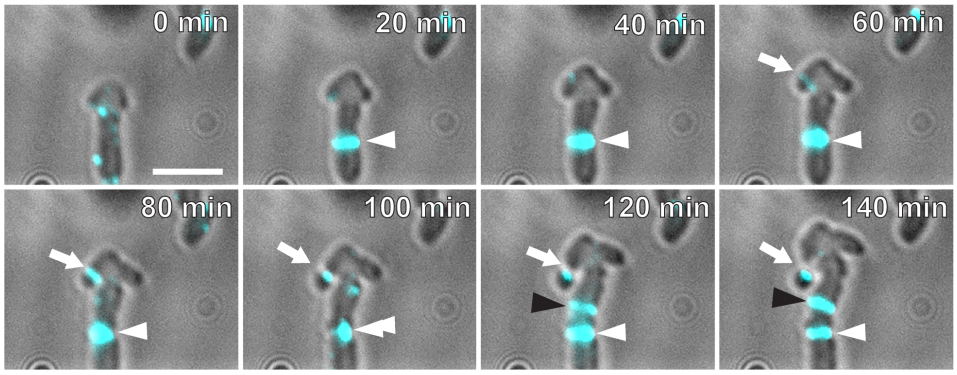

Figure 3.11 FtsZ-GFP localizes in multiple rings in *ΔpodJ*$_{At}$. FtsZ-GFP (cyan) localizes in multiple "Z-rings" (white arrowhead, black arrowhead). FtsZ-GFP also localizes to an ectopic division site producing a small spherical cell (white arrow).

The multiple "rings" observed via FtsZ-GFP and FtsA-GFP localization may contribute to the partial constriction phenotype in many *ΔpodJ$_{At}$* cells with multiple constrictions observed by SEM (Figure 3.2 C and D, Figure 3.4). That some septal rings (indicated by FtsA- and FtsZ-GFP localization) do not constrict indicates that *ΔpodJ$_{At}$* cells have a defect in division.

3.3.1.5 *ΔpodJ$_{At}$* displays a division and timing defect resulting in anucleate minicells

Multiple Z-rings and division events producing small cells in *ΔpodJ$_{At}$* cells suggest that *ΔpodJ$_{At}$* displays a division timing or placement defect. Indeed, time-lapse images of *ΔpodJ$_{At}$* cells indicate division events sometimes produce small cells that do not undergo further growth or division (Figure 3.12 A). 4',6-diamidino-2-phenylindole (DAPI) staining in *ΔpodJ$_{At}$* was compared to WT (Figure 3.12 B). Only <1% of WT cells were shorter than 1 μm and did not stain with DAPI. In contrast, 6% of *ΔpodJ$_{At}$* were shorter than 1 μm and none of these cells were stained with DAPI. Thus, the very small *ΔpodJ$_{At}$* cells observed are anucleate and cannot grow. The occurrence of anucleate *ΔpodJ$_{At}$* cells may partially account for the decrease in CFU of *ΔpodJ$_{At}$* in comparison to WT.

3.3.1.6 Comparing *ΔpodJ$_{At}$* to *S. meliloti ΔpodJ1*

PodJ was previously studied in a related member of the Rhizobiales, *S. meliloti*. The *S. meliloti ΔpodJ1* strain also displayed morphological defects such as the branching observed here. *ΔpodJ1* also exhibited a motility defect and different growth and morphology phenotypes on different media (49). We observed that *ΔpodJ$_{At}$* also has a partial motility defect in comparison to WT as observed in a soft agar flagellar motility assay (Figure 3.13). The *ΔpodJ$_{At}$* flagellar motility phenotype may reflect that deviations from rod shape decrease the efficiency of flagella motility in *ΔpodJ$_{At}$*. Or, flagellar subunit transcription may be lower as shown for deletion of *podJ1* in *S. meliloti* (49).

S. meliloti ΔpodJ1 was less viable when grown on LB plates with low salt (LBLS) (49); however, growth in LBLS did not impact the viability of *ΔpodJ$_{At}$* (Figure 3.14). Growth in PYE medium improved *S. meliloti ΔpodJ1* morphology and FtsZ-GFP localization phenotypes (49); however, growth in PYE did not impact the viability of *ΔpodJ$_{At}$* (Figure 3.14). A quantitative assessment of hundreds of cells revealed that growth in PYE medium only partially complemented the morphology phenotype of *ΔpodJ$_{At}$*, reducing the frequency of cells with deviations from rod-shape versus *ΔpodJ$_{At}$* grown in LB (Table 3.4). In contrast to *S. meliloti ΔpodJ1*, *ΔpodJ$_{At}$* cells grown in PYE displayed abnormal FtsZ-GFP localization, including peripheral sidewall localization (Figure 3.15 A-E) and multiple ring localization (Figure 3.15 F), in addition to normal polar and mid-cell FtsZ-GFP localization (Figure 3.15 G-H). WT cells grown in PYE displayed WT FtsZ-GFP localizations (13), including polar and midcell FtsZ-GFP localization (Figure 3.15 I-K). The differences between the phenotypes of *A. tumefaciens ΔpodJ$_{At}$* and the *S. meliloti ΔpodJ1* suggest that the details of PodJ activity may be different in these two organisms. Muropeptide analysis indicates 64% of peptide stems are cross-linked in *A. tumefaciens*

peptidoglycan compared to 43% of peptide stems in *S. meliloti* peptidoglycan (18). The high degree of peptidoglycan cross-linking in *A. tumefaciens* may account for the insensitivity of $\Delta podJ_{At}$ to low-salt media.

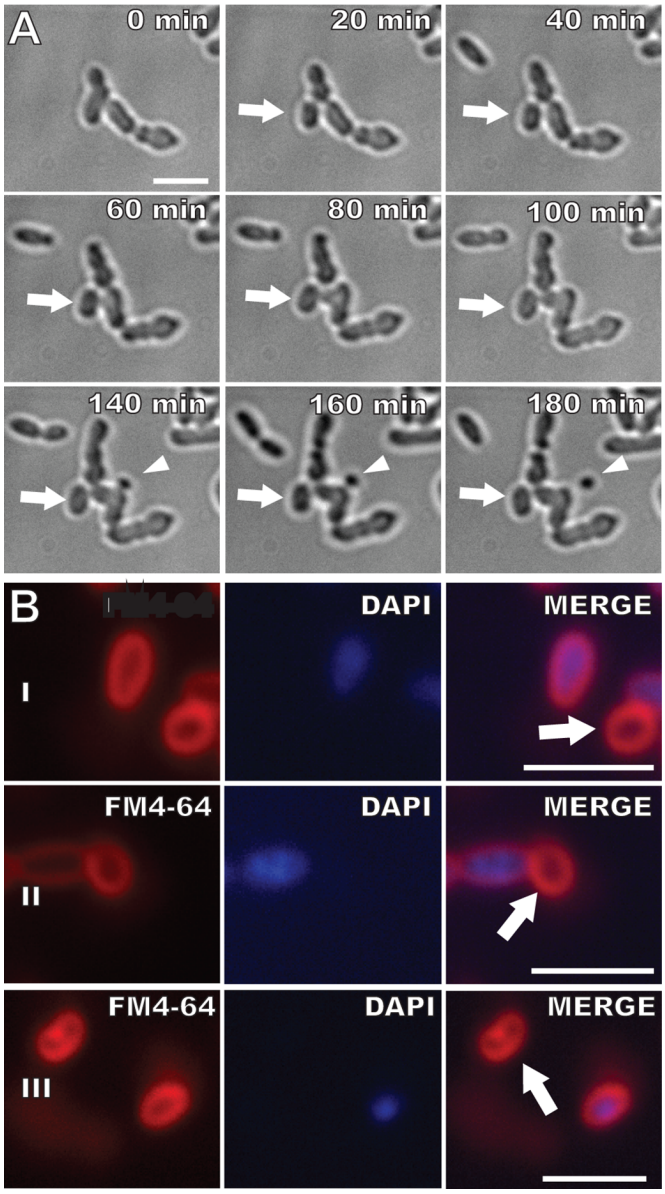

Figure 3.12 *ΔpodJ*$_{At}$ produces non-growing and small anucleate cells. A) Arrow indicates a cell that does not grow or divide, and arrowhead indicates a spherical minicell. B) FM4-64 and DAPI staining. Some small *ΔpodJ*$_{At}$ cells do not stain with DAPI (white arrows). Scale bars, 3 µm.

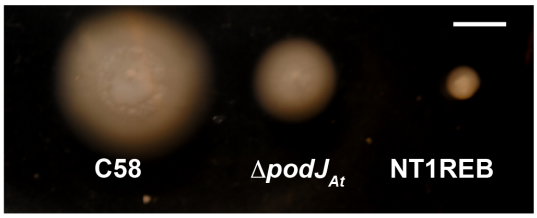

Figure 3.13 Motility of *ΔpodJ*$_{At}$ is intermediate between WT and flagella minus strains. Soft agar motility assay of *ΔpodJ*$_{At}$, WT, and NT1REB (bald/flagella minus strain). Scale bar, 0.5 cm.

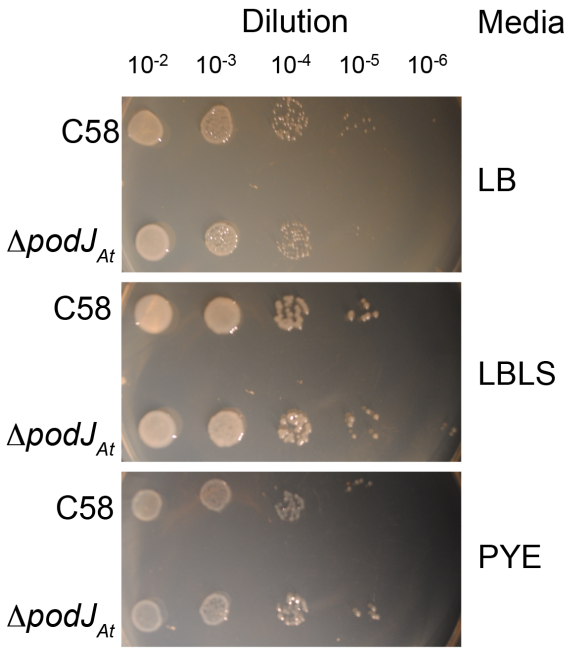

Figure 3.14 *ΔpodJ*$_{At}$ grows equally as well as WT on LB, LBLS, and PYE solid media. Growth on LB, LBLS, and PYE plates for the indicated dilutions is compared for the WT and *ΔpodJ*$_{At}$ strain.

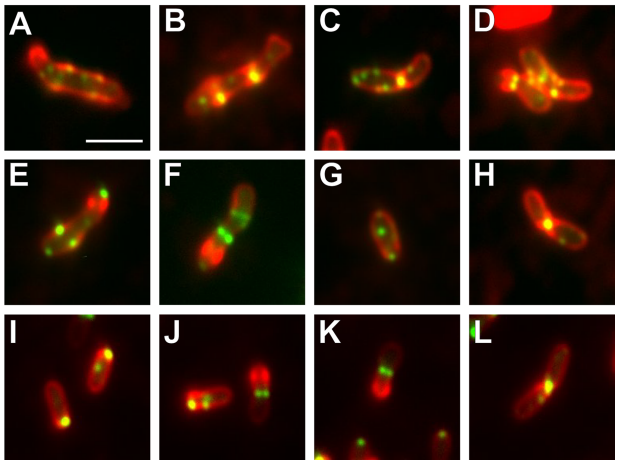

Figure 3.15 *ΔpodJ*$_{At}$ cells grown in PYE display abnormal FtsZ-GFP localization, whereas C58 FtsZ-GFP localization is normal. In *ΔpodJ*$_{At}$ cells grown in PYE, FtsZ-GFP localizes in multiple peripheral foci (A-E), multiple rings (F), and polar (G) and midcell foci (I). In WT cells grown in PYE, FtsZ-GFP localizes to the poles (J-K) and at the midcell (L-I). Scale bar indicates 3 µm.

Table 3.4 Growth in PYE partially complements the *ΔpodJ$_{At}$* morphology phenotype.
Frequency of *ΔpodJ$_{At}$* and WT cells grown in LB and PYE displaying different morphologies are compared for LB and PYE.

	LB		PYE	
	WT	*ΔpodJ$_{At}$*	WT	*ΔpodJ$_{At}$*
Rod-shaped	96 %	60 %	97 %	78 %
Multiple constriction/bent	4 %	29 %	3 %	17 %
Branched/ swollen	0 %	8 %	0 %	4 %
Minicell	0 %	3 %	0 %	1 %
Number of cells counted	283	262	295	340

3.4 DISCUSSION

In WT *A. tumefaciens*, GFP-PodJ$_{At}$ continuously localizes to non-growing old poles. Importantly, GFP-PodJ$_{At}$ also localizes to growth poles later in the cell cycle when such poles must begin to transition into old poles just before cell division (21). Here, in the absence of PodJ$_{At}$ growth poles fail to transition to old, non-growth poles and ectopic growth poles are initiated; these results support that PodJ$_{At}$ is a critical factor in normal polar growth in *A. tumefaciens.* Further, the aberrant localization of FtsA- and FtsZ-GFP in *ΔpodJ$_{At}$* cells suggests that PodJ$_{At}$ indirectly impacts both the timing and site of Z-ring assembly. Z-ring function also is altered in *ΔpodJ$_{At}$* as Z-rings form but often do not result in septation and production of daughter cells. The alterations from WT morphology in *ΔpodJ$_{At}$*, can be seen most readily in dynamic time-lapse videos, where initially morphologically normal-looking cells grow and divide, and then stochastically give rise to cells with dramatic deviations from rod shape.

In WT, a growth pole arises at the septal sites in siblings following cell division. The growth pole is active for most of cell cycle, then, prior to cell division, it transitions to an old pole (Figure 1.1). In *ΔpodJ$_{At}$* ectopic growth poles arise in three different contexts. First, some growth poles fail to transition to old poles and, after cell division, continue to elongate. Second, adjacent growth poles are formed when a single growth pole splits into two growth poles; splitting of the growth pole occurs simultaneously with

broadening and splitting of the localization of new pole identity factor $PopZ_{At}$-GFP. Third, some growth poles arise apparently *de novo* from the cell sidewall.

How might $PodJ_{At}$ function? The failure of growth poles to transition and the initiation of ectopic growth poles in the absence of $PodJ_{At}$ suggest that $PodJ_{At}$, (directly or indirectly) acts as a negative regulator of polar growth in *A. tumefaciens.* The constant localization of GFP-$PodJ_{At}$ to non-growing poles in WT at first glance supports this suggestion (67). Alternatively, $PodJ_{At}$ might act positively to regulate unknown negative regulators of polar growth. In *C. crescentus* other developmental factors rely on $PodJ_{CC}$ for proper localization (47, 48, 71). Late in the *A. tumefaciens* cell cycle GFP-$PodJ_{At}$ localizes to small foci at growth poles (Figure 1.1, (67)) perhaps reflecting a need for a threshold level of $PodJ_{AT}$ to allow localization of other factors to begin the growth pole-old pole transition (discussed further below).

Development of branched morphologies in *A. tumefaciens* and related organisms has been described previously (20, 25, 27, 72, 73). Now that we know *A. tumefaciens* grows by polar growth (13, 14, 18) we may better understand these earlier phenotypes. In rod shaped-organisms such as *E. coli,* which elongate by uniform insertion of new cell envelope material throughout the sidewall, mutations that inhibit cell division cause filamentous morphologies due to continued elongation without cell division (31, 40, 74). When polar-growing members of the Rhizobiales are subject to mutations inhibiting cell division, branching morphologies result instead (20, 43). As $PodJ_{At}$ is a polar localizing factor we expected its loss to alter polar growth. However, we also observed defective cell division and abnormal branching occurs in its absence, phenotypes observed for treatments designed to affect cell division in the Rhizobiales (20, 34). Given that polar growth and cell division must be intimately connected, potentially the defects in cell division and branching in $\Delta podJ_{At}$ are secondary consequences resulting from its primary defect in polar growth.

The induction of ectopic polar growth in $\Delta podJ_{At}$ indicates that there are factors that actively promote or organize polar growth. Indeed, $PopZ_{At}$, localizes to the growth pole of young cells, and relocalizes to the growth poles of recently divided daughter cells immediately after septation (67). In *C. crescentus*, $PopZ_{Cc}$ is initially localized to the stalked pole where it anchors the chromosome. In response to chromosome replication, a second $PopZ_{Cc}$ focus forms at the flagellar pole as part of the chromosome segregation mechanism (51, 64). *C. crescentus* $PopZ_{Cc}$ continuously localizes to old poles and temporarily to new poles as they transition to old poles (50, 51). In contrast, the localization of $PopZ_{At}$-GFP exclusively to growth poles in WT (21) and to all observed types of ectopic growth poles in $\Delta podJ_{At}$ supports that $PopZ_{At}$ localization consistently indicates new growth pole localization.

Besides localizing to the Z-ring as expected, *A. tumefaciens* FtsA-GFP and FtsZ-GFP localize to the growth pole in WT (13, 14, 63). That *A. tumefaciens* FtsZ may play additional roles in cell growth is supported by studies in the related Rhizobiale *S.*

meliloti, where overexpression of FtsZ-GFP caused significant morphological deviations from rod shape (20). In *ΔpodJ$_{At}$* FtsA-GFP localized in bipolar, sub-polar, and peripheral foci, as well as extra Z-rings, patterns not observed in WT. In *ΔpodJ$_{At}$* there were significantly less FtsA-GFP and FtsZ-GFP foci at the growth poles, and the intensity of polar localization was weaker than in WT; thus, abnormalities in polar growth due to the loss of one factor likely impact the localization of other polar localizing factors such as FtsA and FtsZ. A greater proportion of *ΔpodJ$_{At}$* cells display Z-ring FtsZ-GFP and FtsA-GFP localization than WT cells. SEM of *ΔpodJ$_{At}$* revealed that many cells displayed multiple shallow constrictions and very few tight constrictions that would be expected for septation. Thus, *ΔpodJ$_{At}$* cells initiate Z-rings readily, but such rings are defective or slowed in contraction and division.

We propose that the most likely cause of the division defect in *ΔpodJ$_{At}$* is the failure of PodJ$_{At}$ to direct the transition of the growth pole to an old pole. This hypothesis is supported by our observation that the new pole-localizing factor, PopZ$_{At}$, fails to leave the growth pole in *ΔpodJ$_{At}$.* In WT PopZ$_{At}$ leaves the growth pole and reappears in both sibling cells at the post-septal sites (67). To enable immediate and equal localization in both siblings, PopZ$_{At}$ likely arrives at the septum just prior to septation, possibly playing a late cell-cycle role in Z-ring function. Our earlier time-lapse studies could not distinguish whether PopZ$_{At}$ migrates or is degraded and then resynthesized and targeted to new growth poles (67). The results herein suggest that PopZ$_{At}$ migrates to the septum in WT cells.

Alternatively, PodJ$_{At}$ may have an indirect effect on cell division via its potential requirement for the polar localization and function of additional cell cycle regulators. In *C. crescentus,* PodJ$_{Cc}$ is part of a complex network of proteins, including PleC$_{Cc}$, that activates the master cell cycle regulator CtrA specifically in the nascent swarmer cell compartment and newborn swarmer cell (75). Indeed, in *S. meliloti*, PodJ1 is suggested to play a critical role in PleC$_{Sm}$ signaling, and PleC$_{Sm}$ is essential for cell viability and may play a role in cell division (49). By analogy, PodJ$_{At}$ may influence the localization or activity of components of the cell division and development regulatory pathway, for example PleC (Atu0982) or DivK (Atu1296) (76). Additionally, PodJ$_{At}$ is longer (1248 aa) than PodJ$_{Cc}$ (974 aa), and may have additional functions. Note the two proteins are only 23 % identical, but both contain a large cytoplasmic domain with numerous coiled-coil regions that may mediate interactions with other polar factors.

Polar development factors in the alphaproteobacteria can have distinct roles in both polar development and proper cell division. In *C. crescentus,* TipN is critical in positioning new-pole structures such as flagella, and exerts an influence on cell division by interacting with ParA at the new pole during chromosome segregation.(77). Similarly, PodJ$_{At}$ may impact polar growth and cell division independently.

Relatively little is known about the factors that regulate polar growth and many questions remain to be addressed (16). Regarding PodJ$_{At}$, does it function as a negative

or positive regulator of polar growth? What factors keep $PodJ_{At}$ forever at old poles? How is polar growth machinery disassembled at the growth pole? Does $PodJ_{At}$ interact with $PopZ_{At}$? Does the arrival of $PodJ_{At}$ directly signal the departure of $PopZ_{At}$? Do *A. tumefaciens* homologs of cell cycle regulators depend on $PodJ_{At}$ for polar localization and play a role in transition of a growth pole into an old pole? Understanding the regulation of cellular asymmetry that mediates unipolar growth in *A. tumefaciens* will likely uncover new paradigms for bacterial morphogenesis.

4 FtsZ and cell division in *Agrobacterium tumefaciens*

4.1 Summary

In *E. coli*, a mutation in the GTP binding site of FtsZ (FtsZN207C) leads to decreased GTP binding and hydrolysis, and expression of the mutant FtsZ in WT cells leads to a growth defect. In this study, I make the analogous mutation in *A. tumefaciens* full-length FtsZ (Atu2086A), FtsZN211C. I observe morphological phenotypes in *A. tumefaciens* cells expressing FtsZN211C indicating a block in cell division. I present evidence that the FtsZ variant expressed, FtsZN211C-GFP, accumulates to higher levels than WT FtsZ-GFP under the same expression conditions. I also characterize the midcell-only localization of the non-essential shorter FtsZ, FtsZ2 (Atu4673) in *A. tumefaciens* cells, and confirm earlier results indicating that FtsZ2 is dispensible for normal growth.

4.2 Introduction

4.2.1.1 FtsZ biology in rod-shaped organisms

Rod-shape morphology in bacteria can arise from different modes of growth in different organisms. In well-studied models such as *E. coli,* rod shape arises from uniform insertion of new cell envelope material in the sidewall of the cell, resulting in cell elongation (15). In contrast, members of the Rhizobiales, such as *Agrobacterium* and *Brucella,* elongate by addition of new cell wall material at one pole of the cell (13, 14, 16-18).

Bacterial cell division in rod-shaped organisms depends on the formation of a cytokinetic ring at the midcell. FtsZ is a tubulin homolog essential for cell division in most bacteria. FtsZ assembles into a ring structure at midcell, recruiting many peptidoglycan synthesis and remodeling enzymes required for septation (12). FtsZ sequences generally consist of a short N-terminal domain, an FtsZ core domain containing sequence features associated with GTP binding and hydrolysis, a spacer region, and a conserved C-terminal domain (78) (Figure 4.1 A and B). FtsZ assembles into protofilaments, and polymerization is dependent on GTP binding (79) (Figure 3.1D). FtsZ protofilaments are initially straight. GTP hydrolysis promotes both protofilament curvature and disassembly. Protofilament curvature could be involved in septation (80). Expression of FtsZ dimer-interface mutants can cause dominant negative impacts. In *E. coli*, expression of the FtsZ dimer interface mutant N207C at three times WT FtsZ levels causes growth defects. N207C exhibited ~74% of WT GTP binding, and ~2% of WT GTPase activity. It is thought that the mutant protein assembles into FtsZ protofilaments with WT FtsZ and impairs the function of WT FtsZ (81) (Figure 4.1 E).

Unsurprisingly, FtsZ expression levels are subject to strict regulation in *E. coli* (82) and *C. crescentus* (83). The ClpX protease degrades *E. coli* FtsZ in vitro in an ATP-dependent fashion. The ClpX N-terminus binds the 18 C-terminal residues of FtsZ. ClpX appears to preferentially degrade polymerized FtsZ. Deletion of ClpX results in slower turnover of FtsZ in vivo, and overexpression of ClpX causes filamentation, presumably because FtsZ

is no longer present to orchestrate cell division (84). FtsZ is also a target of the ClpXP and ClpAP proteases in *C. crescentus*, where it is degraded preferentially in newborn swarmer cells. ClpXP and ClpAP degradation of FtsZ requires the FtsZ conserved C-terminal core (85). Some members of the Rhizobiales, a family of which *A. tumefaciens* is a member, and includes other polar-growing organisms, have two *ftsZ* genes in their genomes. Maximum Likelihood phylogenetic analysis indicated that the shorter *ftsZ* genes (*ftsZ2*) of the Rhizobiaceae and Phyllobacteriaceae duplicated before the divergence of these families. The short FtsZ2 proteins do not contain the conserved C-terminal core of other FtsZ proteins, or the extended C-terminal linker common in Alpha-proteobacterial full-length FtsZ proteins. Phylogenetic analysis of *ftsZ* also indicates that a separate *ftsZ* gene duplication event occurred in the Bradyrhizobiaceae (78).

As described in the introduction, despite apparent morphological similarity, rod-shaped organisms that grow by unipolar growth display different growth defects in response to blocks in cell division than cells that grow by uniform insertion of new cell wall material throughout the sidewall. To better understand the role of the short FtsZ encoded protein, I monitored the localization of FtsZ2-GFP and the phenotype of *ΔftsZ2*. I then studied the impact of predicted dominant negative alleles of the essential full-length *ftsZ* on *A. tumefaciens* growth and morphology.

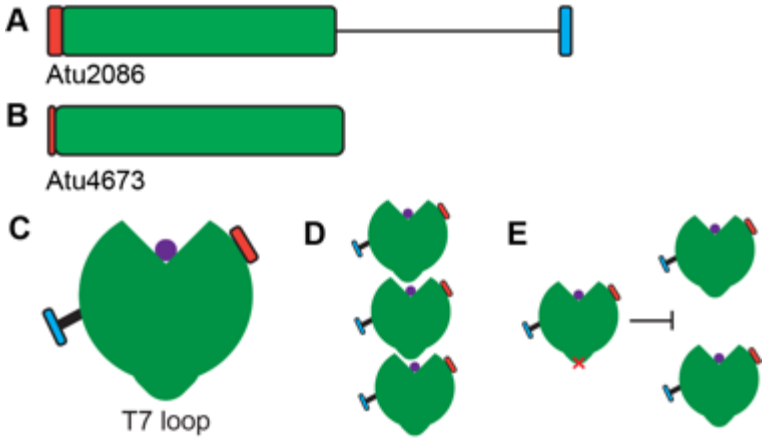

Figure 4.1 Sequence features of the two FtsZ sequences in *A. tumefaciens*. A) The full length FtsZ contains the N-terminal domain (orange), the FtsZ core tubulin homologous domain (green), a C-terminal spacer (line) and a conserved C-terminal domain (blue) implicated in interactions with Z-ring associated proteins in other organisms. B) FtsZ2 contains a shorter ? N-terminal domain (orange), and the FtsZ core domain (green). C) Schematic of the FtsZ structure, with the GTP/GDP binding site cleft on top (GTP/GDP represented by a purple dot) and the T7 loop on bottom. Other domains are color-coded as in A). D) A schematic of FtsZ polymerization. GTPase active sites are constituted by the binding site cleft of one subunit and the T7 loop of the adjacent subunit. E) Schematic of the inhibition of normal FtsZ polymerization by the presence of the N211C mutant (indicated with red 'X'-mark).

4.3 UNIQUE MATERIALS AND METHODS

4.3.1.1 Bacterial strains and growth conditions

Strains and plasmids used in this study are described in Table 3.1. Cells were grown in AB minimal medium pH 5.5 in 19 C and induced with IPTG as described previously (2, 13).

4.3.1.2 Gel electrophoresis and Western blotting

Sodium dodecyl sulfate polyacrylamide gel electrophoresis was performed using the Laemmli method (86). Volumes of cultures predicted to contain 10^8 cells based on OD600 measurements were pelleted. Whole cell pellets were boiled for 10 minutes in loading buffer. 10% Laemmli gels were run and stained with Coomassie stain or transferred to Polyvinylidine fluoride (PVDF) membranes for Western blotting as described previously (87). Chicken anti-GFP antibody was used to label GFP.

Table 3.1 Strains and plasmids used in this study

Strains	**Relevant genotype**	**Source**
XL1 Blue	*E. coli* cloning strain, *endA1 gyrA96*(nal^R) thi-1 *recA1 relA1* lac glnV44 F'[::Tn10 *proAB*+ *lacIq* Δ(*lacZ*)M15] hsdR17(rK-mK+), Tet^R.	Lab stock
C58	wild-type *A. tumefaciens* strain C58	Lab stock
ΔftsZ2	C58, *ΔftsZ2,* using pJAF044, Kan^R	This work
Plasmids	**Relevant genes and construction information**	**Source**
pSRK-Km	Broad host-range, lac inducible, Kan^R	(69)
pBluescript II SK	Phagemid, Carb^R	Stratagene
pJAF039	pSRK-Km with *ftsZ2-GFP*, lac-inducible, Kan^R	This work
pJAF044	pBSKII+ with *sacB*, Carb^R, Kan^R	This work
pJZ207	pSRK-Km with *ftsZ-GFP*, lac-inducible, Kan^R	(13)
pJAF051	pSRK-Km with *ftsZN211C-GFP*, lac-inducible, Kan^R	This work

4.4 RESULTS

4.4.1.1 FtsZN211C-GFP accumulates to higher levels than WT FtsZ-GFP, and its expression causes deviation from rod-shape in A. tumefaciens

I wondered whether a predicted GTPase deficient mutant version of FtsZ would interfere with normal FtsZ function in *A. tumefaciens*. Additionally, I wished to observe the impact of such a mutation on FtsZ localization. To answer these questions, I created the Asparagine to Cysteine mutation in *A. tumefaciens* FtsZ, N211C, corresponding to the *E. coli* FtsZ dominant negative GTPase mutation, N207C.

FtsZN211C-GFP expression in *A. tumefaciens* results in severe morphological abnormalities. In rich media (LB) at high temperatures (28°C), cells expressing

FtsZN211C-GFP are elongated and branched. FtsZN211C-GFP localizes to multiple peripheral foci instead of the polar and midcell localizations seen for WT FtsZ-GFP (Figure 4.3 A-H). In minimal acidic media (AB pH 5.5) at low temperatures (19°C), branched cells are also observed (Figure 4.3 J, N, P). However, cells additionally display a swollen phenotype, and FtsZN211C-GFP localizes at the swollen areas (Figure 4.3 I-L). In many cells, the swelling phenotype is most severe at the midcell, and FtsZ localizes in ring-like structures (Figure 4.3 I, N). In some cells, FtsZN211C-GFP may localize to multiple rings, assuming midcell foci indicate complete rings (Figure 4.3 K, N).

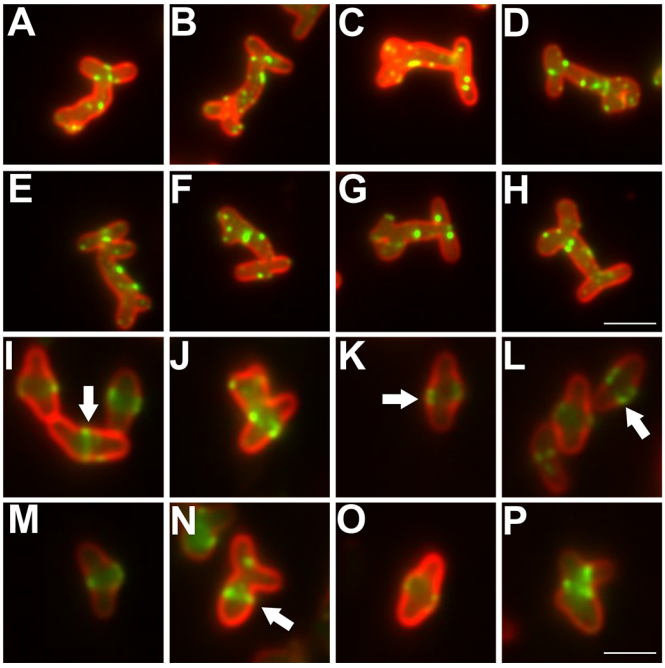

Figure 4.3 Expression of FtsZ-GFP point mutants causes morphological phenotypes in *A. tumefaciens*. A-H) Cells expressing FtsZN211C-GFP in LB at 28 C display branching phenotypes with mutant FtsZ localized in peripheral foci. I-P) Cells expressing FtsZN211C-GFP in AB minimal media, pH 5.5 at 19 C display branching, midcell bulges, and FtsZ localized at bulges. Ring-like structures indicated with white arrowheads. Scale bars indicate 3 μm.

Because overexpression of FtsZ can cause morphological deviations from normal shape in bacteria (19, 20), I next asked whether the morphological abnormalities observed were at least partly due to overexpression of the mutant FtsZ. To test this, I compared WT and N211C FtsZ-GFP levels in an anti-GFP Western blot. When these two proteins were expressed from the same lac promoter on the same low copy-number plasmid backbone, FtsZN211C-GFP was present in larger quantities than WT FtsZ-GFP, whether in LB at 28°C (Figure 4.4 lanes A-D) or AB pH 5.5 at 19°C (Figure 4.4 lanes E-H). Coomassie staining of an identically-loaded gel indicates that less protein was loaded in lanes E-H (corresponding to cells grown in AB pH 5.5) than in lanes A-D (corresponding to cells grown in LB), though the protein loading within lanes A-D or E-H is internally consistent. Thus, comparisons between the quantities of FtsZ-GFP variants in lanes B and D or lanes F and H is valid (Figure 4.4 B).

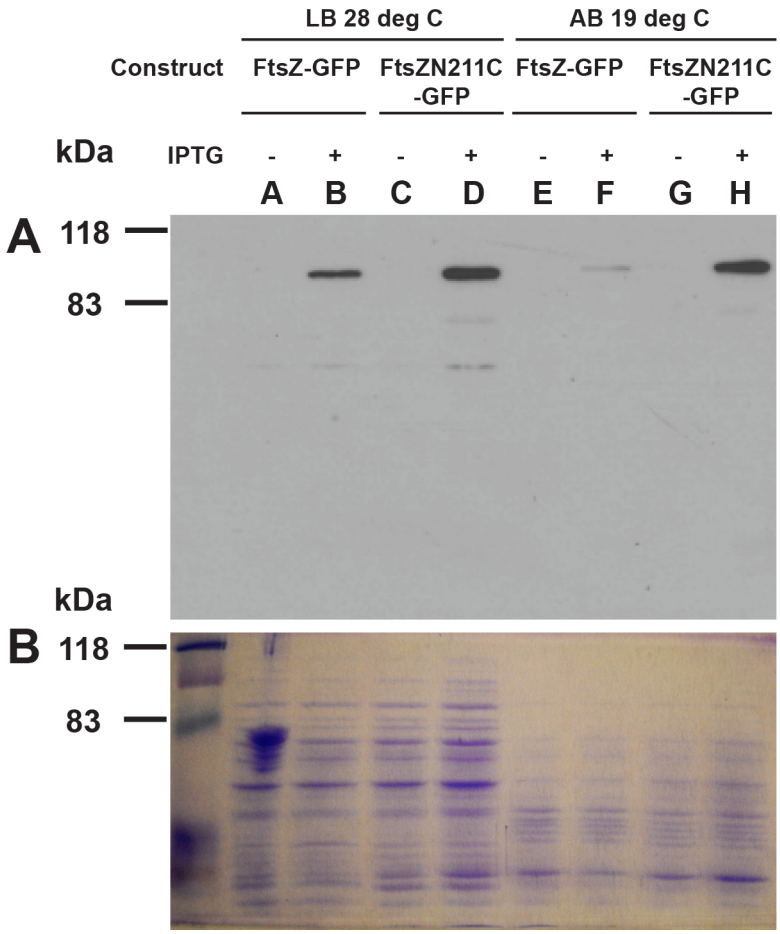

Figure 4.4 FtsZN211C-GFP is present at higher levels than WT FtsZ-GFP expressed from the same promoter under either LB or AB growth conditions. A) Anti-GFP Western blot of FtsZ-GFP variants expressed in *A. tumefaciens.* Growth conditions, expression construct, and presence or absence of IPTG are indicated above the blot image. Growth in LB at 28°C indicated in lanes A-D, growth in AB pH 5.5 at 19°C indicated in lanes A-D. Primary antibody is anti-GFP. B) Coomassie stain of identically-loaded gel, showing overall lower loading of proteins from whole cell extracts of cultures grown in AB medium.

4.4.1.2 FtsZ2 is dispensible for growth in A. tumefaciens and localizes to the midcell

In *A. tumefaciens,* full-length FtsZ-GFP localizes to polar and sidewall foci in addition to the midcell localization seen predominantly in other species such as *E. coli* and *B. subtilis* (13). To probe the distinct features of FtsZ biology in *A. tumefaciens*, I also examined the localization of a shorter FtsZ encoded in the genome of several Rhizobiaceae (78) (FtsZ2, Figure 4.1 B). FtsZ2 lacks canonical FtsZ sequence features, such as the C-terminal domain required for association with other Z-ring proteins in organisms such as *E. coli* (78, 88).

FtsZ2-GFP was expressed from a lac-inducible promoter on a low copy-number plasmid. Localization patterns of FtsZ2-GFP were counted for 847 cells. FtsZ2-GFP displayed diffuse cytoplasmic localization in 95% of cells (Figure 4.5 A). In 5% of cells, FtsZ2-GFP localized to the midcell (Figure 4.5 A, white arrowheads). I next measured the cell

lengths for cells displaying diffuse and midcell FtsZ2-GFP localization. Cell lengths for cells displaying each FtsZ2-GFP localization pattern were measured, and Gaussian kernel density estimates for the cell length distributions were plotted (Figure 4.5 B). To facilitate comparison between the diffuse localization cell length density approximation (n=803) and the mid-cell localization cell length density approximation (n=44), the y-values for the density curves were normalized to 1.0 for each category (Figure 4.5 B). Cells with diffuse FtsZ2-GFP localization tended to be shorter (mean=1.48 mm, median=1.42 mm) than cells with mid-cell FtsZ2-GFP localization (mean=2.40 mm, median=2.39 mm).

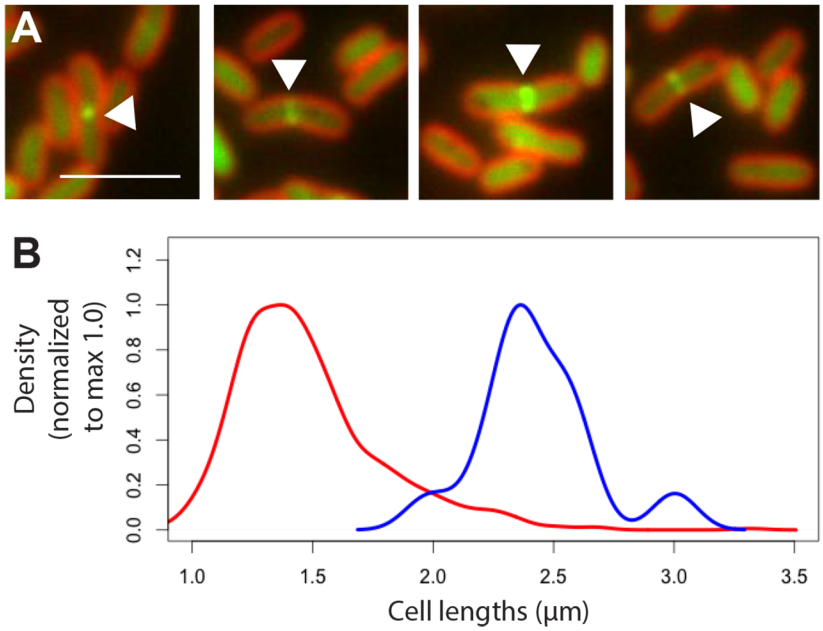

Figure 4.5 FtsZ2 localizes in the cytoplasm in shorter cells and at the midcell in longer cells in *A. tumefaciens*. A) Representative images of FtsZ2-GFP localization in WT A. tumefaciens. Cells with midcell localization are indicated with white arrows. Midcell localization occurred in 5% of cells, and cytoplasmic localization occurred in 95% of cells. Scale bar indicates 3 µm. B) Cell length distribution of cells with cytoplasmic FtsZ2-GFP localization (red) is skewed towards shorter cells than the cell length distribution of cells with midcell FtsZ2-GFP localization (blue). Y-axis of cell length distributions is normalized to 1.0 (n=803 for cytoplasmic, n=44 for midcell).

I next verified that deletion of FtsZ2 in *A. tumefaciens* did not impact cell growth or morphology, as reported for *R. meliloti* (20). Indeed, *DftsZ2* cells stained with FM4-64 displayed morphology similar to WT cells (Figure 4.6 A), and grew similarly to WT cells in LB media as measured by OD600 (Figure 4.6 B).

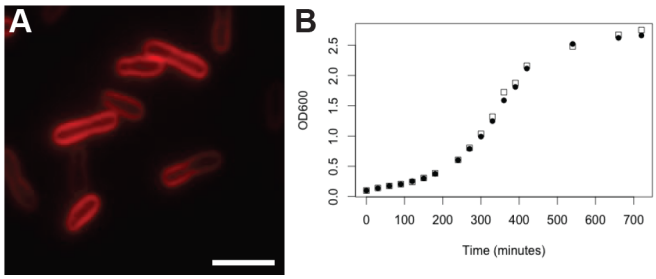

Figure 4.6 Deletion of the FtsZ2 does not impact cell growth or morphology in *A. tumefaciens*. A) Morphologically-normal ΔftsZ2 cells stained with FM4-64. Scale bar indicates 3 μm. B) OD600 growth curve comparing increase in optical density for WT A. tumefaciens (□) and ΔftsZ2 (•).

4.5 Discussion

FtsZ2, lacking the C-terminal domain present in full-length FtsZ, does not localize to the poles in *A. tumefaciens*. Potentially this sequence feature of the full-length FtsZ is required for polar localization. In other organisms such as *E. coli*, the C-terminal domain is necessary for FtsZ to interact with other proteins such as FtsA (88). In *A. tumefaciens*, FtsA localizes at the growth pole in addition to the midcell. Perhaps FtsA or other unknown factors are responsible for anchoring FtsZ localization to the poles via interaction with the C-terminus of FtsZ.

Chloroplasts, which likely evolved from cyanobacterial endosymbionts, also encode two *ftsZ* sequences in their genomes (89). Studies of the filament morphologies and dynamics of these proteins expressed separately and together in yeast indicate that one FtsZ forms the protofilament backbone for chloroplast division and the other FtsZ influences Z-ring remodeling (90). Of the two FtsZ sequences observed in *A. tumefaciens*, the essential FtsZ1 may be iinvolved in cytokinesis, and the non-essential FtsZ2 may be involved in modulating FtsZ1 dynamics under some growth conditions that were not investigated herein

Also of note is the disruption of normal morphology by expression of FtsZN211C-GFP. Expression of WT FtsZ-GFP using the same growth conditions and the same lac-inducible expression vector does not result in these phenotypes (13). I hypothesize that severe morphological phenotype observed due to ectopic expression of FtsZN211C-GFP is due to a deficiency in proteolytic turnover of FtsZN211C-GFP. The ClpX protease degrades *E. coli* FtsZ in vitro in an ATP-dependent fashion. ClpX N-terminus binds the 18 C-terminal residues of FtsZ. ClpX appears to preferentially degrade polymerized FtsZ. Deletion of ClpX results in slower turnover of FtsZ in vivo, and overexpression of ClpX causes filamentation, presumably because FtsZ is no longer present to orchestrate cell division (84). FtsZ is also a target of the ClpXP and ClpAP proteases in *C. crescentus*, where it is degraded preferentially in newborn swarmer cells. ClpXP and ClpAP degradation of FtsZ requires the FtsZ conserved C-terminal core (85). The genome of *A. tumefaciens* also encodes ClpA (Atu1364), ClpP (ClpP1: Atu1627, ClpP2: Atu1258, ClpP3: Atu2270), and ClpX (Atu1259) homologs. Given that the FtsZN207C mutant in *E. coli* (corresponding to the FtsZN211C mutant reported here) is deficient in polymerization (81) the analogous

Agrobacterium point mutant FtsZN211C may also interfere with polymerization. In addition, the likely occlusion of the C-terminus by GFP in the FtsZN211C-GFP construct may interfere with normal degradation of the mutant protein by ClpXP/AP, resulting in the accumulation of FtsZN211C-GFP as illustrated in Fig. 3.1 and shown by the over accumulation of this protein by Western analysis. Such over accumulation likely competes and interferes with normal FtsZ function, resulting in the observed morphological deviations from rod shape.

5 MORPHOLOGICAL EFFECTS OF BLOCKING CELL DIVISION WITH ANTIBIOTICS IN *AGROBACTERIUM TUMEFACIENS*

5.1 INTRODUCTION

5.1.1.1 Peptidoglycan synthesis and structure in gram-negative bacteria

The plasma membrane of gram-negative bacteria is surrounded by a murein sacculus, which is composed of a covalently closed peptidoglycan mesh. The shape of the peptidoglycan mesh controls the shape of bacterial cells, an assertion supported by the observation that purified peptidoglycan sacculi maintain the shape of the bacterial cells from which they are derived (91).

Peptidoglycan precursors are β 1→4 linked N-acetyl-muramic acid and N-acetyl glucosamine with pentapeptide stems. The terminal three amino acids of the pentapeptide stem are an amino acid with L- and D- centers, commonly meso-Di-amino pimelic acid (DAP) and two distal D-amino acids, commonly D-ala. The peptidoglycan mesh consists of glycan strands composed of β 1→4 linked N-acetyl-muramic acid and N-acetyl glutamic acid, cross-linked to other adjacent glycan strands via the peptide stems (91). Canonical peptide stem cross-linking is via transpeptidation of the D- center of the third amino acid in one stem to the fourth D-amino acid in the adjacent stem. Such D,D-transpeptidation reaction is catalyzed by class A (bifunctional enzymes which also display transglycosylase activity) and B (monofunctional) Penicillin Binding Proteins (PBPs) (92).

L,D-transpeptidases can also cross-link peptidoglycan via the non-canonical transpeptidation of adjacent L- and D- amino acids from different glycan strands, though these cross-links are not always present in all organisms with peptidoglycan. L,D-transpeptidases were first characterized in organisms such as *Mycobacterium tuberculosis* and *Enterococcus faecium* (93, 94).

5.1.1.2 Probing the function of PG synthesis enzymes using antibiotics

Penicillin and its derivatives, such as carbenicillin, inhibit the D,D-transpeptidase activity of PBPs. In E. coli, treatment with sub-lethal doses of beta-lactam derivatives results in cells displaying morphological defects. Treatment by the antibiotic mecillinam results in swollen ovoid cells that eventually lyse. Biochemical evidence indicates that mecillinam specifically targets the D,D-transpeptidase activity of PBP2 (95-97). The swollen cell morphology is interpreted to indicate a defect in sidewall peptidoglycan cross-linking, further indicating that PBP2 plays a role in sidewall peptidoglycan cross-linking. Treatment of *E. coli* with beta-lactam derivatives such as furazlocillin, pipercillin, and ampicillin, which specifically target the D,D-transpeptidase activity of PBP3, results in cells with filamentous morphology (95, 97). Filamentous cell morphology occurs in many cases where cell division is blocked, such as overexpression or depletion of FtsZ (74, 98). The filamentous cell morphology of carbenicillin-treated *E. coli* cells is interpreted to indicate that PBP3 is involved in peptidoglycan cross-linking at the septum. It is also

notable that L,D-transpeptidases are associated with resistance to penicillin derivatives such as ampicillin in organisms like *M. tuberculosis* and *E. faecium* (93, 94).

5.1.1.3 PG synthesis enzymes, polar growth, and cell division in *A. tumefaciens*

L,D-transpeptidases may play an important role in polar growth in *A. tumefaciens*. A search for homologs of peptidoglycan synthesis proteins encoded in the *A. tumefaciens* genome identified two D,D-Transpeptidases which are more similar to the cell division PBP FtsQ (PBP3) of *E. coli* than the elongation-associated PBP2, and 14 possible L,D-transpeptidase genes (14). L,D/3-3 cross-linked stem peptides make up ~45% of the peptide cross-links in the murein sacculus of *A. tumefaciens* (18). Fluorescently labeled D-Ala derivatives, which are incorporated into peptidoglycan by an L,D-transpeptidase-catalyzed exchange reaction (99, 100), localize at the growth pole and midcell of *A. tumefaciens*, as does a GFP-fusion to a predicted periplasmic L,D-Transpeptidase (14).

Though many proteins localize to the growing pole of *A. tumefaciens*, the components essential for polar growth remain unknown. Moreover, many peptidoglycan synthesis enzymes could well be redundant due to the presence of several homologous sequences for a given enzyme class. Beta lactam antibiotics target many different enzymes in any given species based on their affinity for specific classes of active sites; indeed, it is hypothesized that the multi-target nature of beta lactams is part of what makes them a useful therapeutic (101). As a result, treatment of cells with antibiotics and observation of the resulting phenotype can serve as a chemical genetics technique to probe the function of an entire class of genes, instead of the labor-intensive approach of attempting to knock out each gene in a family in a given species (102). When biochemical data indicate that antibiotics specifically inhibit certain enzymes, morphological effects of sub-lethal antibiotic doses implicate targeted enzymes in maintenance of normal morphology.

Given the hypothesis that L,D-transpeptidases are important in cross-linking peptidoglycan during polar growth, we predicted that inhibition of L,D-transpeptidases with a sub-lethal concentration of antibiotic would result in *A. tumefaciens* cells with defects in polar morphology. Members of the carbapenem family of antibiotics, such as imipenem, can inhibit L,D-transpeptidases in *Mycobacterium* and *Enterococcus* (103-106).

5.2 Unique materials and methods

5.2.1.1 Growth conditions for antibiotics treatment

WT cells were grown in overnights in LB at 28° C. For imipenem treatment, cells were diluted to OD_{600} = 0.1 in LB and grown for four hours at 28° C with 250 ng/mL imipenem. For carbenicillin treatment, cells diluted into AB medium pH 5.5 and grown with 30 μg/mL carbenicillin for 20 hours.

5.3 Results

SEM of carbenicillin-treated cells displayed the midcell bulges visible in light micrographs (Figure 5.1). Bulges had constrictions at their centers, resulting in the

appearance of two overlapping bulges. Some cells had protrusions resembling wild type cell poles extending from the midcell region.

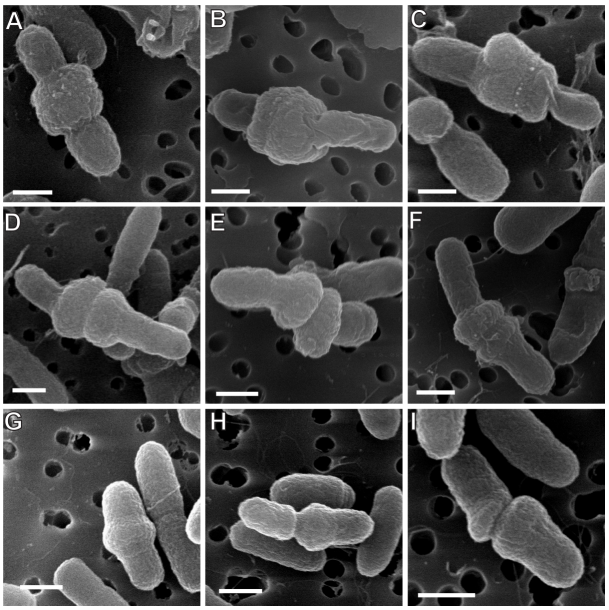

Figure 5.1 Carbenicillin-treated cells exhibit midcell bulges and other variations in width. Cells treated with 30 ug/mL carbenicillin display single midcell bulges (A-C), dual midcell bulges separated by a constriction (D-F), and smaller midcell bulges (G-H). In some cells, the angle of the constriction between bulges deviates from perpendicular to the long axis of the cell (I). Scale bars indicate 0.5 μm.

SEM of imipenem-treated cells indicated branched morphologies in addition to midcell bulges seen for carbenicillin-treated cells (Figure 5.2). Overall, the Imipenem-treated cells were variable in cell width.

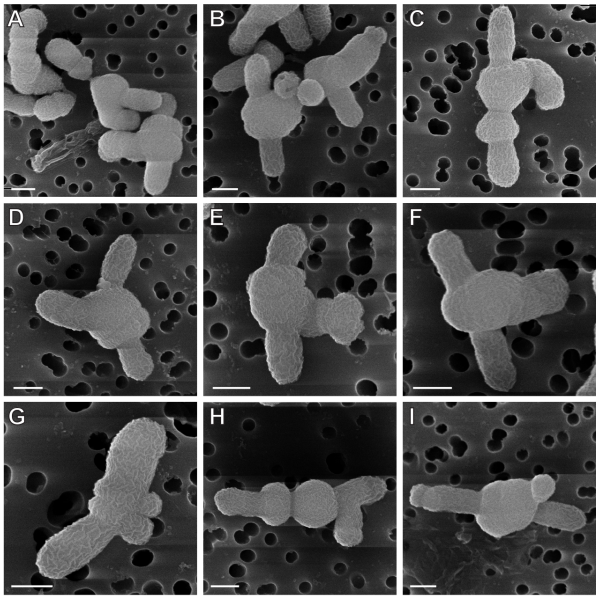

Figure 5.2 Imipenem-treated cells exhibit bulges and branches. Imipenem-treated cells display bulges, constrictions, and branched morphologies (A), often with multiple branches extending from a single bulge (B), cells with multiple bulges and branches (C), and various configurations of the aforementioned features (D-I). Scale bars indicate 0.5 μm.

5.4 Discussion

The appearance of branches in imipenem-treated cells indicates that polar growth is, to some extent, still functional in these cells. It is difficult to imagine a process other than polar growth that could give rise to structures so resembling normal growth poles that are observed in imipenem-treated cells. By definition, sub-lethal doses of antibiotics allow some growth to continue in antibiotic-susceptible cells (107). Cell treatment with the sub-lethal concentrations of imipenem used here may therefore leave a fraction of PG cross-linking enzymes involved in polar growth uninhibited, allowing polar growth to continue. *A. tumefaciens* and other related polar-growers often display a branching phenotype as a result of an arrest in polar growth (see section 1.4). Thus, the morphological phenotypes seen in imipenem-treated cells are likely due to a block in cell division in these cells, and not a complete block in polar growth.

Interpretation of these data is limited by the fact that the enzymes inhibited by carbenicillin and imipenem in *A. tumefaciens* are unknown. The hypothesis that imipenem inhibits L,D-transpeptidases in *A. tumefaciens* is based on the fact that carbapenems inhibit L,D-transpeptidases in other bacteria (93, 104, 105) and the assumption that enzymes similar in sequence and activity are inhibited by the same drugs. Additionally, several enzymes generally categorized as PBPs can be targets of carbenicillin and other penicillin derivatives. Besides D,D-transpeptidase PBPs, D,D-carboxypeptidases and endopeptidases are also classified as PBPs, and could also be inhibited by penicillin derivatives (108). Thus, the morphological response of *A. tumefaciens* to carbenicillin treatment could also partly be due to the inhibition of D,D-carboxypeptidases or endopeptidases. Future biochemical work would verify that imipenem inhibits *A. tumefaciens* L,D-transpeptidases, or that carbenicillin inhibits cross-linking D,D-transpeptidases instead of peptide stem-remodeling D,D-carboxypeptidases or endopeptidases. This could be accomplished by treating *A. tumefaciens* protein extracts with labeled antibiotic derivatives and identifying the proteins which bind to the labeled antibiotics using electrophoresis (109) and mass spectrometry (110).

Questions also remain regarding PG structure and composition in the morphologically abnormal antibiotic-treated cells. For instance, is the midcell bulge observed in carbenicillin-treated cells the result of reduced PG cross-linking? This question could be addressed through structural analysis of the sacculus in carbenicillin-treated cells (111). I would predict that the frequency of cross-linked muropeptides in carbenicillin-treated cells would be lower than the frequency of cross-linked muropeptides observed in untreated cells.

6 SUMMARY: POLAR GROWTH AND CELL DIVISION ARE INTER-RELATED PROCESSES IN *AGROBACTERIUM TUMEFACIENS*

Here, we explore facets of cell growth and division unique to the polar-growing Rhizobiales. Under certain growth conditions, blocking cell division in these polar-growing organisms results in a branching morphology distinct from the filamentation observed in sidewall-growers with a defect in cell division. The bases for branch formation in a polar-growing organism remains unclear. In detailed time-lapse analysis of branch formation in the $\Delta podJ_{At}$ strain, we observe what appears to be splitting of one growth pole into two adjacent growth poles, as well as growth of a branch point from a point along the sidewall of the cell.

In the filamentous bacterium *Streptomyces coelicolor,* polar growth is organized by a protein complex called the polarisome. The coiled-coil protein DivIVA localizes in cytoplasmic foci at growth poles and is a scaffold for the cell wall assembly components involved in polar growth. Notably *A. tumefaciens* does not possess an obvious DivIVA homolog. In *S. coelicolor*, which undergoes branching, DivIVA foci split, resulting in deposition of small DivIVA foci at future branch sites (112). Thus, it is thought that fragmentation of a landmark protein complex critical for the assembly of polar growth machinery is an essential step in the formation of branch points.

A. tumefaciens may possess a similar complex composed of cytoplasmic scaffolding proteins, transmembrane proteins, and periplasmic proteins involved in peptidoglycan synthesis and creation of new cell envelope material at the growth pole. In WT cells, this complex must assemble at the division site, producing two growth poles after septation completes. In cells blocked for cell division it is possible that the polar growth complex splits from one existing growth pole into two in a manner analogous to DivIVA focus splitting in *S. coelicolor*. Alternatively, in cells that form an ectopic growth pole from a position along the sidewall of the cell, a new growth pole may be produced at the aborted division site.

The formation of branched morphologies upon division inhibition in the Rhizobiales suggests a linkage between polar growth and cell division in these organisms. Studies of $podJ_{At}$ indicated that this polar-localizing factor may play a role in cell division. $\Delta podJ_{At}$ displayed abnormal localization of FtsZ-GFP and FtsA-GFP, produced anucleate minicells, and displayed the branching morphologies indicative of a block in cell division in *A. tumefaciens*. How would a polar-localizing factor impact cell division? Based on knowledge of the *C. crescenstus* and *S. meliloti* cell cycles, I propose that the division defect in $\Delta podJ_{At}$ is due to altered expression of genes involved in cell division. A *podJ* deletion strain in *S. meliloti* is deficient in polar localization of the cell cycle response regulator DivK (49), and a similar strain in *C. crescentus* is deficient in the polar localization of the histidine kinase PleC (48). In *C. crescentus*, both PleC and DivK are part of a regulatory circuit which controls phosphorylation and thus transcriptional activity of the master cell-cycle regulator CtrA (47). The CtrA regulon includes genes involved in critical cell-cycle processes such as DNA replication, cell wall remodeling, and

cell division (21). . Future studies should address the roles of CtrA, PleC, and DivK in Agrobacterium. Because of deficiencies in polar localization of cell cycle regulators, expression levels of cell division proteins may be misregulated in *ΔpodJ$_{At}$*, resulting in division defects.

Indeed, deletion of *podJ1* in *S. meliloti* disrupts transcription of several genes, including *ftsZ2* and genes in the *min* locus. *ftsZ2* transcription is higher in the *ΔpodJ1* strain than in WT (49). This suggests that FtsZ2 transcription is regulated and that it plays some role in normal cell division, even if its deletion does not result in an observable phenotype under normal laboratory growth conditions. Overexpression of FtsZ2 in *R. meliloti* causes the formation of branched and swollen morphologies, suggesting that overexpression of FtsZ2 interferes with normal cell division in the Rhizobiaceae (20), likely by interfering with FtsZ1. Potentially, the increased expression of FtsZ2 in the *ΔpodJ1* strain of *S. meliloti* is partially involved in the division defect observed in that organism.

Potentially many of the morphological phenotypes in *ΔpodJ$_{At}$* are due to defects in cell division stemming from a disruption in cell-cycle dependent gene expression. Equally likely are two other explanations: either the defect in cell division is a consequence of a defect in growth pole-old pole transition, or PodJ$_{At}$ plays a role in polar development independent or related to its role in cell division. Another polar landmark protein in the alpha-proteobacteria that is involved simultaneously in cell division and polar development is TipN in *C. crescentus* (77)*,* and ongoing studies in the Zambryski lab suggests it is a critical factor in Agrobacterium polar growth.

Dynamic live-cell imaging reveals that one phenotype of *ΔpodJ$_{At}$* is a defect in the growth pole-old pole transition: growth poles continue to grow after division, instead of transitioning to old poles. PopZ$_{At}$-GFP localizes exclusively to growing poles in WT *A. tumefaciens*, and to ectopic growth poles in *ΔpodJ$_{At}$*. Therefore, PopZ$_{At}$-GFP serves as a marker for polar growth processes. In the normal cell cycle of *A. tumefaciens*, PopZ$_{At}$-GFP relocalizes from the growth pole of a divisional cell to the two growth poles in sibling cells produced by the division event. Though this process occurs too rapidly to observe with current live-cell imaging techniques, PopZ$_{At}$-GFP and other polar growth factors may localize to the midcell during septation and are functionally involved in cell division. As a result, eviction of these polar growth factors from a growth pole may be crucial for cell division. A defect in growth pole eviction concomitant with the growth pole-old pole transition may therefore cause a defect in cell division.

Further work will continue to characterize the role of *A. tumefaciens* polar development factors in polar growth and cell division. What is the phenotype of a PopZ$_{At}$ knockout? A third sequence in the *A. tumefaciens* genome is annotated as FtsZ (Atu4215). A report in *S. meliloti* that sought to identify cell-cycle regulated genes by comparing the transcriptome at different phases of the cell cycle, identified this ORF as a cell-cycle regulated gene (113). Is this third *A. tumefaciens* FtsZ (Atu4215) sequence expressed, and what role does it play in cell division? A transposon sequencing experiment

identified *A. tumefaciens* FtsA as non-essential (114). Is there another gene whose product serves to tether FtsZ to the membrane in *A. tumefaciens*?

7 REFERENCES

1. **Zupan J**, **Muth TR**, **Draper O**, **Zambryski P**. 2000. The transfer of DNA from *Agrobacterium tumefaciens* into plants: a feast of fundamental insights. Plant Journal **23**:11–28.

2. **Aguilar J**, **Zupan J**, **Cameron TA**, **Zambryski PC**. 2010. *Agrobacterium* type IV secretion system and its substrates form helical arrays around the circumference of virulence-induced cells. Proc Natl Acad Sci USA **107**:3758–3763.

3. **Aguilar J**, **Cameron TA**, **Zupan J**, **Zambryski P**. 2011. Membrane and Core Periplasmic *Agrobacterium tumefaciens* Virulence Type IV Secretion System Components Localize to Multiple Sites around the Bacterial Perimeter during Lateral Attachment to Plant Cells. mBio **2**:e00218–11–e00218–11.

4. **Demchick P**, **Koch AL**. 1996. The permeability of the wall fabric of *Escherichia coli* and *Bacillus subtilis*. J Bacteriol **178**:768–773.

5. **Scheurwater EM**, **Burrows LL**. 2011. Maintaining network security: how macromolecular structures cross the peptidoglycan layer. FEMS Microbiol Lett **318**:1–9.

6. **Baron C**, **Llosa M**, **Zhou S**, **Zambryski PC**. 1997. VirB1, a component of the T-complex transfer machinery of *Agrobacterium tumefaciens*, is processed to a C-terminal secreted product, VirB1. J Bacteriol **179**:1203–1210.

7. **Bohne J**, **Yim A**, **Binns AN**. 1998. The Ti plasmid increases the efficiency of *Agrobacterium tumefaciens* as a recipient in virB-mediated conjugal transfer of an IncQ plasmid. Proc Natl Acad Sci USA **95**:7057–7062.

8. **Fullner KJ**. 1998. Role of *Agrobacterium* virB genes in transfer of T complexes and RSF1010. J Bacteriol **180**:430–434.

9. **Vollmer W**, **Bertsche U**. 2008. Murein (peptidoglycan) structure, architecture and biosynthesis in *Escherichia coli*. Biochim Biophys Acta **1778**:1714–1734.

10. **Typas A**, **Banzhaf M**, **Gross CA**, **Vollmer W**. 2011. From the regulation of peptidoglycan synthesis to bacterial growth and morphology. Nature Publishing Group **10**:123–136.

11. **Bernhardt TG**, **de Boer P**. 2003. The *Escherichia coli* amidase AmiC is a periplasmic septal ring component exported via the twin-arginine transport pathway. Mol Microbiol **48**:1171–1182.

12. **Lutkenhaus J**, **Pichoff S**, **Du S**. 2012. Bacterial cytokinesis: From Z ring to

divisome. Cytoskeleton **69**:778–790.

13. **Zupan JR**, **Cameron TA**, **Anderson-Furgeson J**, **Zambryski PC**. 2013. Dynamic FtsA and FtsZ localization and outer membrane alterations during polar growth and cell division in *Agrobacterium tumefaciens.* Proc Natl Acad Sci USA **110**:9060–9065.

14. **Cameron TA**, **Anderson-Furgeson J**, **Zupan JR**, **Zik JJ**, **Zambryski PC**. 2014. Peptidoglycan synthesis machinery in *Agrobacterium tumefaciens* during unipolar growth and cell division. mBio **5**:e01219–14–e01219–14.

15. **Blaauwen Den T**, **de Pedro MA**, **Nguyen-Distèche M**, **Ayala JA**. 2008. Morphogenesis of rod-shaped sacculi. FEMS Microbiol Rev **32**:321–344.

16. **Cameron TA**, **Zupan JR**, **Zambryski PC**. 2015. The essential features and modes of bacterial polar growth. Trends Microbiol **23**:347–353.

17. **Brown PJB**, **Kysela DT**, **Brun YV**. 2011. Polarity and the diversity of growth mechanisms in bacteria. Semin Cell Dev Biol **22**:790–798.

18. **Brown PJB**, **de Pedro MA**, **Kysela DT**, **Van der Henst C**, **Kim J**, **De Bolle X**, **Fuqua C**, **Brun YV**. 2012. Polar growth in the Alphaproteobacterial order Rhizobiales. Proc Natl Acad Sci USA **109**:1697–1701.

19. **Dai K**, **Lutkenhaus J**. 1992. The proper ratio of FtsZ to FtsA is required for cell division to occur in *Escherichia coli*. J Bacteriol **174**:6145–6151.

20. **Latch JN**, **Margolin W**. 1997. Generation of buds, swellings, and branches instead of filaments after blocking the cell cycle of *Rhizobium meliloti.* J Bacteriol **179**:2373–2381.

21. **Collier J**. 2016. Cell cycle control in Alphaproteobacteria. Curr Opin Microbiol **30**:107–113.

22. **Reisenauer A**, **Kahng LS**, **McCollum S**, **Shapiro L**. 1999. Bacterial DNA methylation: a cell cycle regulator? J Bacteriol **181**:5135–5139.

23. **ZWEIGER G**, **MARCYNSKI G**, **Shapiro L**. 1994. A *Caulobacter* Dna Methyltransferase That Functions Only in the Predivisional Cell. J Mol Biol **235**:472–485.

24. **Wright R**, **Stephens C**, **Shapiro L**. 1997. The CcrM DNA methyltransferase is widespread in the alpha subdivision of proteobacteria, and its essential functions are conserved in *Rhizobium meliloti* and *Caulobacter crescentus*. J Bacteriol **179**:5869–5877.

25. **Kahng LS**, **Shapiro L**. 2001. The CcrM DNA Methyltransferase of *Agrobacterium tumefaciens* Is Essential, and Its Activity Is Cell Cycle Regulated. J Bacteriol **183**:3065–3075.

26. **Wright R**, **Stephens C**, **ZWEIGER G**, **Shapiro L**, **Alley M**. 1996. *Caulobacter* Lon protease has a critical role in cell-cycle control of DNA methylation. Genes & Development **10**:1532–1542.

27. **Su S**, **Stephens BB**, **Alexandre G**, **Farrand SK**. 2006. Lon protease of the alpha-proteobacterium *Agrobacterium tumefaciens* is required for normal growth, cellular morphology and full virulence. Microbiology **152**:1197–1207.

28. **Gur E**. 2013. The Lon AAA+ Protease, pp. 35–51. *In* Regulated Proteolysis in Microorganisms. Springer Netherlands, Dordrecht.

29. **Butala M**, **Žgur-Bertok D**, **Busby SJW**. 2008. The bacterial LexA transcriptional repressor. Cell Mol Life Sci **66**:82–93.

30. **Huisman O**, **D'Ari R**. 1981. An inducible DNA replication-cell division coupling mechanism in E. coli. Nature **290**:797–799.

31. **BI E**, **Lutkenhaus J**. 1993. Cell-Division Inhibitors SulA and MinCD Prevent Formation of the Ftsz Ring. J Bacteriol **175**:1118–1125.

32. **Modell JW**, **Hopkins AC**, **Laub MT**. 2011. A DNA damage checkpoint in *Caulobacter crescentus* inhibits cell division through a direct interaction with FtsW. Genes & Development **25**:1328–1343.

33. **Mo AH**, **Burkholder WF**. 2010. YneA, an SOS-Induced Inhibitor of Cell Division in *Bacillus subtilis*, Is Regulated Posttranslationally and Requires the Transmembrane Region for Activity. J Bacteriol **192**:3159–3173.

34. **Fujiwara T**, **Fukui S**. 1974. Effect of D-Alanine and Mitomycin-C on Cell Morphology of *Agrobacterium tumefaciens*. Journal of General and Applied Microbiology **20**:345–349.

35. **Weart RB**, **Lee AH**, **Chien A-C**, **Haeusser DP**, **Hill NS**, **Levin PA**. 2007. A metabolic sensor governing cell size in bacteria. Cell **130**:335–347.

36. **Chien A-C**, **Zareh SKG**, **Wang YM**, **Levin PA**. 2012. Changes in the oligomerization potential of the division inhibitor UgtP co-ordinate *Bacillus subtilis* cell size with nutrient availability. Mol Microbiol **86**:594–610.

37. **Hill NS**, **Buske PJ**, **Shi Y**, **Levin PA**. 2013. A Moonlighting Enzyme Links *Escherichia coli* Cell Size with Central Metabolism. PLoS Genet **9**:e1003663–14.

38. **Beaufay F**, **Coppine J**, **Mayard A**, **Laloux G**, **De Bolle X**, **Hallez R**. 2015. A NAD-dependent glutamate dehydrogenase coordinates metabolism with cell division in *Caulobacter crescentus*. EMBO J **34**:1786–1800.

39. **Beaufay F**, **De Bolle X**, **Hallez R**. 2016. Metabolic control of cell division in α-proteobacteria by a NAD-dependent glutamate dehydrogenase. Communicative & Integrative Biology 00–00.

40. **de Boer PA**, **Crossley RE**, **Rothfield LI**. 1989. A division inhibitor and a topological specificity factor coded for by the minicell locus determine proper placement of the division septum in *E. coli*. Cell **56**:641–649.

41. **Cha JH**, **Stewart GC**. 1997. The divIVA minicell locus of *Bacillus subtilis*. J Bacteriol **179**:1671–1683.

42. **Patrick JE**, **Kearns DB**. 2008. MinJ (YvjD) is a topological determinant of cell division in *Bacillus subtilis*. Mol Microbiol **70**:1166–1179.

43. **Cheng J**, **Sibley CD**, **Zaheer R**, **Finan TM**. 2007. A *Sinorhizobium meliloti minE* mutant has an altered morphology and exhibits defects in legume symbiosis. Microbiology **153**:375–387.

44. **Skerker JM**, **Laub MT**. 2004. Cell-cycle progression and the generation of asymmetry in *Caulobacter crescentus*. Nat Rev Micro **2**:325–337.

45. **Holtzendorff J**, **Reinhardt J**, **Viollier PH**. 2006. Cell cycle control by oscillating regulatory proteins in *Caulobacter crescentus*. Bioessays **28**:355–361.

46. **Brilli M**, **Fondi M**, **Fani R**, **Mengoni A**, **Ferri L**, **Bazzicalupo M**, **Biondi EG**. 2010. The diversity and evolution of cell cycle regulation in alpha-proteobacteria: a comparative genomic analysis. BMC Syst Biol **4**.

47. **Viollier PH**, **Sternheim N**, **Shapiro L**. 2002. Identification of a localization factor for the polar positioning of bacterial structural and regulatory proteins. Proc Natl Acad Sci USA **99**:13831–13836.

48. **Hinz AJ**, **Larson DE**, **Smith CS**, **Brun YV**. 2003. The *Caulobacter crescentus* polar organelle development protein PodJ is differentially localized and is required for polar targeting of the PleC development regulator. Mol Microbiol **47**:929–941.

49. **Fields AT**, **Navarrete CS**, **Zare AZ**, **Huang Z**, **Mostafavi M**, **Lewis JC**, **Rezaeihaghighi Y**, **Brezler BJ**, **Ray S**, **Rizzacasa AL**, **Barnett MJ**, **Long SR**, **Chen EJ**, **Chen JC**. 2012. The conserved polarity factor PodJ1 impacts multiple cell envelope-associated functions in *Sinorhizobium meliloti*. Mol Microbiol **84**:892–920.

50. **Ebersbach G**, **Briegel A**, **Jensen GJ**, **Jacobs-Wagner C**. 2008. A self-associating protein critical for chromosome attachment, division, and polar organization in *Caulobacter*. Cell **134**:956–968.

51. **Bowman GR**, **Comolli LR**, **Zhu J**, **Eckart M**, **Koenig M**, **Downing KH**, **Moerner WE**, **Earnest T**, **Shapiro L**. 2008. A polymeric protein anchors the chromosomal origin/ParB complex at a bacterial cell pole. Cell **134**:945–955.

52. **Laloux G**, **Jacobs-Wagner C**. 2013. Spatiotemporal control of PopZ localization through cell cycle-coupled multimerization. J Cell Biol **201**:827–841.

53. **Montoya AL**, **Chilton MD**, **Gordon MP**, **Sciaky D**, **Nester EW**. 1977. Octopine and nopaline metabolism in *Agrobacterium tumefaciens* and crown gall tumor cells: role of plasmid genes. J Bacteriol **129**:101–107.

54. **Sambrook J**, **Fritsch EF**, **Maniatis T**. 1989. Molecular cloning: a laboratory manual, 2nd ed. Cold Spring Harbor Laboratory Press, Cold Spring Harbor, NY.

55. **Blomfield IC**, **Vaughn V**, **Rest RF**, **Eisenstein BI**. 1991. Allelic exchange in *Escherichia coli* using the *Bacillus subtilis sacB* gene and a temperature-sensitive pSC101 replicon. Mol Microbiol **5**:1447–1457.

56. **van Teeffelen S**, **Wang S**, **Furchtgott L**, **Huang KC**, **Wingreen NS**, **Shaevitz JW**, **Gitai Z**. 2011. The bacterial actin MreB rotates, and rotation depends on cell-wall assembly. Proc Natl Acad Sci USA **108**:15822–15827.

57. **Garner EC**, **Bernard R**, **Wang W**, **Zhuang X**, **Rudner DZ**, **Mitchison T**. 2011. Coupled, circumferential motions of the cell wall synthesis machinery and MreB filaments in *B. subtilis*. Science **333**:222–225.

58. **Domínguez-Escobar J**, **Chastanet A**, **Crevenna AH**, **Fromion V**, **Wedlich-Söldner R**, **Carballido-López R**. 2011. Processive movement of MreB-associated cell wall biosynthetic complexes in bacteria. Science **333**:225–228.

59. **Braña AF**, **Manuel-Benjamin M**, **C H**. 1982. Mode of cell wall growth of *Streptomyces antibioticus*. FEMS Microbiol Lett **13**:231–235.

60. **Miguélez EM**, **Martín C**, **Manzanal MB**, **Hardisson C**. 1992. Growth and morphogenesis in *Streptomyces*. FEMS Microbiol Lett **100**:351–359.

61. **Meniche X**, **Otten R**, **Siegrist MS**, **Baer CE**, **Murphy KC**, **Bertozzi CR**, **Sassetti CM**. 2014. Subpolar addition of new cell wall is directed by DivIVA in mycobacteria. Proc Natl Acad Sci USA **111**:E3243–E3251.

62. **Thanky NR**, **Young DB**, **Robertson BD**. 2007. Unusual features of the cell cycle in mycobacteria: Polar-restricted growth and the snapping-model of cell division.

Tuberculosis **87**:231–236.

63. **Ma X**, **Sun Q**, **Wang R**, **Singh G**, **Jonietz EL**, **Margolin W**. 1997. Interactions between heterologous FtsA and FtsZ proteins at the FtsZ ring. J Bacteriol **179**:6788–6797.

64. **Bowman GR**, **Perez AM**, **Ptacin JL**, **Ighodaro E**, **Folta-Stogniew E**, **Comolli LR**, **Shapiro L**. 2013. Oligomerization and higher-order assembly contribute to sub-cellular localization of a bacterial scaffold. Mol Microbiol **90**:776–795.

65. **Laloux G**, **Jacobs-Wagner C**. 2013. How do bacteria localize proteins to the cell pole? J Cell Sci **127**:11–19.

66. **Ptacin JL**, **Gahlmann A**, **Bowman GR**, **Perez AM**, **Diezmann von ARS**, **Eckart MR**, **Moerner WE**, **Shapiro L**. 2014. Bacterial scaffold directs pole-specific centromere segregation. Proc Natl Acad Sci USA **111**:E2046–E2055.

67. **Grangeon R**, **Zupan JR**, **Anderson-Furgeson J**, **Zambryski PC**. 2015. PopZ identifies the new pole, and PodJ identifies the old pole during polar growth in *Agrobacterium tumefaciens*. Proc Natl Acad Sci USA **112**:11666–11671.

68. **Chesnokova O**, **Coutinho JB**, **Khan IH**, **Mikhail MS**, **Kado CI**. 1997. Characterization of flagella genes of Agrobacterium tumefaciens, and the effect of a bald strain on virulence. Mol Microbiol **23**:579–590.

69. **Khan SR**, **Gaines J**, **Roop RM**, **Farrand SK**. 2008. Broad-host-range expression vectors with tightly regulated promoters and their use to examine the influence of TraR and TraM expression on Ti plasmid quorum sensing. Appl Environ Microbiol **74**:5053–5062.

70. **Klüsener S**, **Hacker S**, **Tsai Y-L**, **Bandow JE**, **Gust R**, **Lai E-M**, **Narberhaus F**. 2010. Proteomic and transcriptomic characterization of a virulence-deficient phosphatidylcholine-negative *Agrobacterium tumefaciens* mutant. Mol Genet Genomics **283**:575–589.

71. **Crymes WB**, **Zhang D**, **Ely B**. 1999. Regulation of *podJ* expression during the *Caulobacter crescentus* cell cycle. J Bacteriol **181**:3967–3973.

72. **Fujiwara T**, **Fukui S**. 1972. Isolation of morphological mutants of *Agrobacterium tumefaciens*. J Bacteriol **110**:743–746.

73. **Fujiwara T**, **Fukui S**. 1974. Unidirectional growth and branch formation of a morphological mutant, *Agrobacterium tumefaciens*. J Bacteriol **120**:583–589.

74. **Dai K**, **Lutkenhaus J**. 1991. *ftsZ* is an essential cell division gene in *Escherichia coli*. J Bacteriol **173**:3500–3506.

75. **Curtis PD**, **Brun YV**. 2010. Getting in the loop: regulation of development in *Caulobacter crescentus*. Microbiol Mol Biol Rev **74**:13–41.

76. **Kim J**, **Heindl JE**, **Fuqua C**. 2013. Coordination of Division and Development Influences Complex Multicellular Behavior in *Agrobacterium tumefaciens*. PLoS ONE **8**:e56682–13.

77. **Schofield WB**, **Lim HC**, **Jacobs-Wagner C**. 2010. Cell cycle coordination and regulation of bacterial chromosome segregation dynamics by polarly localized proteins. EMBO J **29**:3068–3081.

78. **Vaughan S**, **Wickstead B**, **Gull K**, **Addinall SG**. 2004. Molecular Evolution of FtsZ Protein Sequences Encoded Within the Genomes of Archaea, Bacteria, and Eukaryota. Journal of Molecular Evolution **58**:19–29.

79. **MUKHERJEE A**, **Lutkenhaus J**. 1994. Guanine Nucleotide-Dependent Assembly of Ftsz Into Filaments. J Bacteriol **176**:2754–2758.

80. **Erickson HP**, **Anderson DE**, **Osawa M**. 2010. FtsZ in Bacterial Cytokinesis: Cytoskeleton and Force Generator All in One. Microbiol Mol Biol Rev **74**:504–528.

81. **Redick SD**, **Stricker J**, **Briscoe G**, **Erickson HP**. 2005. Mutants of FtsZ Targeting the Protofilament Interface: Effects on Cell Division and GTPase Activity. J Bacteriol **187**:2727–2736.

82. **Garrido T**, **Sanchez M**, **Palacios P**, **Aldea M**. 1993. Transcription of *ftsZ* oscillates during the cell cycle of *Escherichia coli*. The EMBO J **12**:3957-3965.

83. **Kelly AJ**, **Sackett MJ**, **Din N**, **Quardokus E**. 1998. Cell cycle-dependent transcriptional and proteolytic regulation of FtsZ in Caulobacter. Genes & Development **12:**880-893.

84. **Camberg JL**, **Hoskins JR**, **Wickner S**. 2009. ClpXP protease degrades the cytoskeletal protein, FtsZ, and modulates FtsZ polymer dynamics. Proc Natl Acad Sci USA **106**:10614–10619.

85. **Williams B**, **Bhat N**, **Chien P**, **Shapiro L**. 2014. ClpXP and ClpAP proteolytic activity on divisome substrates is differentially regulated following the *Caulobacter* asymmetric cell division. Mol Microbiol **93**:853–866.

86. **Laemmli UK**. 1970. Cleavage of structural proteins during the assembly of the head of bacteriophage T4. Nature **227**:680–685.

87. **Harlow E**, **Lane D**. 1988. Antibodies: a laboratory manual. Cold Spring Harbor Laboratory, Cold Spring Harbor, NY.

88. **Ma XL**, **Margolin W**. 1999. Genetic and functional analyses of the conserved C-terminal core domain of *Escherichia coli* FtsZ. J Bacteriol **181**:7531–7544.

89. **McFadden GI**. 1999. Endosymbiosis and evolution of the plant cell. Current Opinion in Plant Biology **2**:513–519.

90. **TerBush AD**, **Osteryoung KW**. 2012. Distinct functions of chloroplast FtsZ1 and FtsZ2 in Z-ring structure and remodeling. J Cell Biol **199**:623–637.

91. **Cabeen MT**, **Jacobs-Wagner C**. 2005. Bacterial cell shape. Nat Rev Micro **3**:601–610.

92. **de Pedro MA**, **Cava F**. 2015. Structural constraints and dynamics of bacterial cell wall architecture. Front Microbiol **6**:1–10.

93. **Mainardi J-L**, **Fourgeaud M**, **Hugonnet J-E**, **Dubost L**, **Brouard J-P**, **Ouazzani J**, **Rice LB**, **Gutmann L**, **Arthur M**. 2005. A novel peptidoglycan cross-linking enzyme for a beta-lactam-resistant transpeptidation pathway. J Biol Chem **280**:38146–38152.

94. **Flores AR**, **Parsons LM**, **Pavelka MS**. 2005. Characterization of Novel *Mycobacterium tuberculosis* and *Mycobacterium smegmatis* Mutants Hypersusceptible to β-Lactam Antibiotics. J Bacteriol **187**:1892–1900.

95. **Waxman DJ**, **Strominger JL**. 1983. Penicillin-binding proteins and the mechanism of action of beta-lactam antibiotics. Annu Rev Biochem **52**:825–869.

96. **Spratt BG**, **Pardee AB**. 1975. Penicillin-binding proteins and cell shape in *E. coli*. Nature **254**:516–517.

97. **Spratt BG**. 1975. Distinct penicillin binding proteins involved in the division, elongation, and shape of *Escherichia coli* K12. Proc Natl Acad Sci USA **72**:2999–3003.

98. **Ward JE**, **Lutkenhaus J**. 1985. Overproduction of FtsZ induces minicell formation in *E. coli*. Cell **42**:941–949.

99. **Lupoli TJ**, **Tsukamoto H**, **Doud EH**, **Wang T-SA**, **Walker S**, **Kahne D**. 2011. Transpeptidase-Mediated Incorporation of D-Amino Acids into Bacterial Peptidoglycan. J Am Chem Soc **133**:10748–10751.

100. **Kuru E**, **Hughes HV**, **Brown PJ**, **Hall E**, **Tekkam S**, **Cava F**, **de Pedro MA**, **Brun YV**, **VanNieuwenhze MS**. 2012. In Situ Probing of Newly Synthesized Peptidoglycan in Live Bacteria with Fluorescent D-Amino Acids. Angew Chem Int Ed **51**:12519–12523.

101. **Silver LL**. 2011. Challenges of Antibacterial Discovery. Clinical Microbiology Reviews **24**:71–109.

102. **Denome SA**, **Elf PK**, **Henderson TA**, **Nelson DE**, **Young KD**. 1999. *Escherichia coli* mutants lacking all possible combinations of eight penicillin binding proteins: viability, characteristics, and implications for peptidoglycan synthesis. J Bacteriol **181**:3981–3993.

103. **Mainardi J-L**, **Hugonnet J-E**, **Rusconi F**, **Fourgeaud M**, **Dubost L**, **Moumi AN**, **Delfosse V**, **Mayer C**, **Gutmann L**, **Rice LB**, **Arthur M**. 2007. Unexpected inhibition of peptidoglycan LD-transpeptidase from *Enterococcus faecium* by the beta-lactam imipenem. J Biol Chem **282**:30414–30422.

104. **Lecoq L**, **Bougault C**, **Triboulet S**, **Dubée V**, **Hugonnet J-E**, **Arthur M**, **Simorre J-P**. 2013. Chemical shift perturbations induced by the acylation of *Enterococcus faecium* l,d-transpeptidase catalytic cysteine with ertapenem. Biomol NMR Assign **8**:339–343.

105. **Triboulet S**, **Dubée V**, **Lecoq L**, **Bougault C**, **Mainardi J-L**, **Rice LB**, **Ethève-Quelquejeu M**, **Gutmann L**, **Marie A**, **Dubost L**, **Hugonnet J-E**, **Simorre J-P**, **Arthur M**. 2013. Kinetic Features of L,D-Transpeptidase Inactivation Critical for β-Lactam Antibacterial Activity. PLoS ONE **8**:e67831–9.

106. **Cordillot M**, **Dubee V**, **Triboulet S**, **Dubost L**, **Marie A**, **Hugonnet JE**, **Arthur M**, **Mainardi JL**. 2013. In Vitro Cross-Linking of *Mycobacterium tuberculosis* Peptidoglycan by L,D-Transpeptidases and Inactivation of These Enzymes by Carbapenems. Antimicrob Agents Chemother **57**:5940–5945.

107. **Andersson DI**, **Hughes D**. 2014. Microbiological effects of sublethal levels of antibiotics. Nature Publishing Group 1–14.

108. **Egan AJF**, **Biboy J**, **van't Veer I**, **Breukink E**, **Vollmer W**. 2015. Activities and regulation of peptidoglycan synthases. Phil Trans R Soc B **370**:20150031–20.

109. **ARÁN V**, **TÉBAR AR**. 1984. Labelling of penicillin-binding proteins with a photoreactive peptidoglycan-peptide analogue. Eur J Biochem **144**:613-616.

110. **Chaurand P**, **Luetzenkirchen F**, **Spengler B**. 1999. Peptide and protein identification by matrix-assisted laser desorption ionization (MALDI) and MALDI-post-source decay time-of-flight mass spectrometry. J Am Soc Mass Spectrom **10**:91–103.

111. **Desmarais SM**, **Tropini C**, **Miguel A**, **Cava F**, **Monds RD**, **de Pedro MA**, **Huang KC**. 2015. High-throughput, Highly Sensitive Analyses of Bacterial Morphogenesis Using Ultra Performance Liquid Chromatography. J Biol Chem **290**:31090–31100.

112. **Richards DM**, **Hempel AM**, **Flärdh K**, **Buttner MJ**, **Howard M**. 2012. Mechanistic Basis of Branch-Site Selection in Filamentous Bacteria. PLoS Comput Biol **8**:e1002423–8.

113. **De Nisco NJ**, **Abo RP**, **Wu CM**, **Penterman J**, **Walker GC**. 2014. Global analysis of cell cycle gene expression of the legume symbiont *Sinorhizobium meliloti*. Proc Natl Acad Sci USA **111**:3217–3224.

114. **Curtis PD**, **Brun YV**. 2014. Identification of essential alphaproteobacterial genes reveals operational variability in conserved developmental and cell cycle systems. Mol Microbiol **93**:713–735.